Tailoring the Acoustic Properties of Truss-Core Sandwich Structure

by

Richard Lee

A thesis submitted in conformity with the requirements
for the degree of Master of Applied Science

Graduate Department of Aerospace Science and Engineering
University of Toronto

Tailoring the Acoustic Properties of Truss-Core Sandwich Structure

Richard Lee

Master of Applied Science

Graduate Department of Aerospace Science and Engineering
University of Toronto

2012

Abstract

Undesirable cabin noise has an adverse physiological effect on passengers and crews in an aircraft. In order to reduce the noise level, a passive approach using a truss-core sandwich (TCS) panel as a sound insulator is proposed. Design guidelines and analysis methodologies were developed in order to explore the vibro-acoustic characteristics of TCS structure. Its sound isolation properties can be thereby assessed. Theoretical analyses show that the transmission-loss and sound radiation properties of a TCS structure can be represented by the root-mean-square velocity of its surface, and a beam structure analysis is sufficient to reveal many of the important aspects of TCS panel design. Using finite element analysis, a sensitivity study was performed to create design guidelines for TCS structures. Transmission-loss experiments show that the analytical and numerical analyses correctly predict the trend of TCS structure's vibro-acoustic performance.

Acknowledgments

I would like to thank my adviser, Professor Craig Steeves, for all his support, guidance, insight, and time. His knowledge and advices on my research were an invaluable part of the successful and timely completion of this research. I owe him much gratitude. I would also like to thank the members of the RAC committee members: Professor Alis Ekmekci, Professor Philippe Lavoie, and Professor David Zingg, for reviewing my work and provided me with much helpful and constructive criticism.

General Dynamics Land Systems of Canada (GDLS-C) has been kind to me for letting me to take an educational leave of absence so that I can concentrate on learning and exploring new ideas to solve complex engineering problems at UTIAS. I want to thank Dave Crocker, the Director of Engineering Design and Development at GDLS-C, for making this opportunity possible. I would also like to thank Bombardier Aerospace (BA) for collaborating with us on this research through the NSERC Engage grant program. Special thanks to Andrew Wareing, Stephen Colavincenzo, and Raymond Wong from BA for their support in this program and conducting the acoustic chamber experiments.

The following people had provided me with much support and made this research experience much more enjoyable: Eska Ko for her friendship, support, and proof-reading my thesis. Professor Jean Zu for her support on solving vibration problems. Collins Ogundipe and John Chu for their help at the Multifunctional Structure Lab. George Lau, Nasim Shahbazian, Jenmy Zhang, and Rhea Liem for their lunch-time conversations. All the members of the Sporting UTIAS soccer team for an exciting season of soccer, and Ludwik Sobiesiak for organizing it. People who were involved in the UTIAS Ping Pong ladder and the tournament for making these events successful.

And finally, I would like to thank Dr. Simona Monaco for her constant support throughout my Master degree endeavor. This degree would not have been possible without her encouragement to pursue my dreams, as well as the courage and strength that she has shown me over the years.

Table of Contents

Contents

List of Tables

List of Figures

Chapter 1

Introduction

Cabin acoustic noise is undesirable for passengers and crew on an aircraft. Noise affects the comfort of people on board an aircraft, and also has a physiological effect on people's health, causing noise induced hearing loss (NIHL), sound annoyance, and elevated stress levels of the passengers. After extended exposure to high noise, typically exceeding 60 to 80 decibels (dB) of a weighted sound level, people will start to experience a temporary threshold shift, which is the primary measure of hearing loss. For these reasons, a reduction in cabin noise level has a direct impact on the health of the passengers and flight crew, the performance of an aircraft, and customers' procurement decisions. In order to reduce the acoustic noise level inside an aircraft cabin, the primary and secondary structural elements inside an aircraft must have superior acoustic transmission loss (TL) properties. In addition, these components also need to provide high stiffness with minimum weight in order to maximize an aircraft's performance and ensure the safety of the passengers. One type of such multi-functional material that is capable providing these properties for an aircraft structure is called the truss-core sandwich (TCS) structure, and the main focus of this research is to explore the design methodologies of TCS structures for producing favourable acoustic transmission loss properties in aerospace applications.

1.1 Background

1.1.1 Source of Cabin Noise

Engine noise and the external flow excitation are the two major sources of the acoustic noise inside an aircraft cabin. These acoustic disturbance sources cause pressure fluctuations around the aircraft exterior, creating a forcing field on the aircraft fuselage. This pressure fluctuation then imparts energy on the fuselage skin causing it to vibrate, and the vibrating elastic fuselage surfaces radiate noise into the aircraft interior. Much of the noise that is generated by modern

gas turbine jet engines is directly related to the engine exhaust, and for a high bypass-ratio turbo fan jet engine or a turbo prop jet engine, additional noise is generated by its fan and its propeller respectively. During takeoff, initial climb and landing, a significant amount of noise is generated by the engine. However, during cruise, the dominating cabin acoustic disturbance is caused by the flow-induced pressure fluctuation. As air flow passes the fuselage, a turbulent boundary layer (TBL) is developed. When the aircraft reaches its cruise altitude, the pressure fluctuation and the cabin noise that are associated with the TBL will be elevated because the flight Mach number is increased, while the engine noise is reduced during the cruise condition. Since the cruise condition represents the majority of the flight time, the TBL induced noise is regarded as the most significant source of noise for jet engine aircraft. As an example, when an aircraft is flying at Mach 0.75, at an altitude of about 30,000 ft, it will generate 130 dB of noise disturbance outside of the fuselage [1]. The transmitted acoustic noise inside an aircraft cabin can vary from 70 dB to 110 dB depending on the type of engine, the flight Mach number, altitude, external flow condition, and the measurement location inside an aircraft cabin. Similar results were found by several other researchers in their studies, as shown in [2-5]. Ribner [6] developed an empirical formula to predict the magnitude of sound pressure levels generated by a range of aircrafts, such as the Boeing 727, Convair 880, and McDonnell-Douglas DC8. For more modern aircraft, such as the Boeing 747, the average cabin noise level for a flight from New York to Heathrow is about 79 dB [7]. As a comparison, the noise generated by city traffic is about 80 dB, which is similar to the cabin noise level. These data suggest that the TBL-induced cabin noise is significant in an aircraft, and it is important to reduce the cabin noise level due to health related issues.

1.1.2 Current Approaches to Reducing Cabin Noise

There are two main methods for reducing the cabin noise level: passive methods and active control methods. Passive methods include structural modifications, material selection, and damping augmentation. In general, active methods use synchrophasing, and the control of acoustic field or the structural vibration to attain active noise cancellation (ANC). The principle of ANC is to create an equal-amplitude and opposite-phase acoustic wave using an array of microphones and speakers or by creating electronically controlled vibrations on a panel. There are number of technical issues related to such systems. First, the reference microphone may pick

up signal from both the primary source (noise) and the secondary source ("anti-noise"), creating a feedback loop, which will amplify the input signal. Also, it may be difficult to achieve high coherence between the reference microphone and the primary source, which is required for good performance of the system. In addition, a large number of speakers and microphones are required to achieve global noise cancellation in an aircraft cabin, which makes this method challenging. On the other hand, using vibration waves on electronically controlled panels requires that all the sensors and actuators function properly over a wide range of operating conditions, and over an extended period of time. The robustness of the system may involve high unit and operating cost of the system over its lifetime if reliability is to be realized. Passive methods do not suffer from the drawbacks of these active systems, and they are the focus of this research project. In particular, the acoustic performance of TCS panels will be analysed and investigated in order to develop a set of methodologies to design this kind of multi-functional sandwich structure for passive control of an aircraft cabin noise level.

1.2 Truss-Core Sandwich

The motivation for using TCS panels to control the cabin noise level stems from their superior mechanical properties and their potential for structural-acoustic optimization. A TCS structure comprises of a pair of strong and stiff face-sheets, laminated to a low-density, light weight core, as shown in Figure 1. In general, the core of a TCS panel is made up of stiff rods arranged in one or more types of lattice structures. In this research, the material used for the rods is a continuous carbon fibre reinforced epoxy resin composite, known as carbon pultruded rods (See Figure 2). Such rods are low in density and high in uniaxial specific stiffness and strength, which is ideal for creating high stiffness sandwich panels with minimal weight penalty. The typical diameters for these carbon rods in a TCS structure are between 0.5 mm to 1.5 mm. Metallic truss members can also be used for TCS panels. However, it was found that the specific stiffness and strength of the all-composite truss core sandwich structure are superior to those of metallic lattice TCS structures [10].

For the same reasons, the material used for the face-sheet in this research is also carbon fibre composite. Bi-directional, plain weaved carbon fibre composite cloth will be used to fabricate the face-sheets for the TCS structure in this research by laminating several layers of carbon fibre cloth together, bonded by a two component mixture of epoxy and hardener. The

resin saturated composite is then vacuum-bagged for curing. The detailed fabrication for a TCS panel comprising carbon fibre face-sheets and a core that is made up of carbon pultruded rods will be discussed in Chapter Four. The three-dimensional, periodic, open-cell lattice structure core not only provides the TCS structure with superior specific bending stiffness and crushing strength, but it may also provide multi-functional capabilities, such as heat insulation, energy absorption, vibration control, and space for wire passage. A number of unit cell designs for the lattice core have shown promising mechanical properties, potential for optimization, and manufacturability.

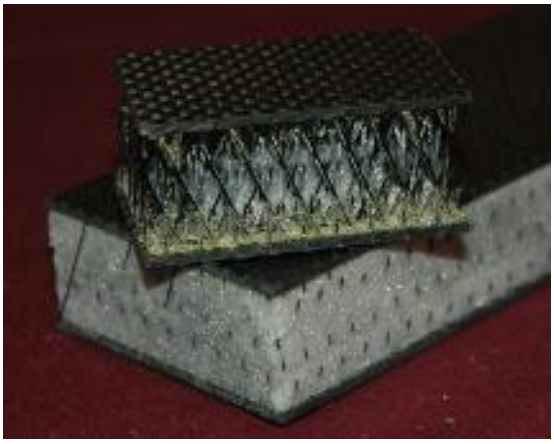

Figure 1. Truss core sandwich (TCS) structure

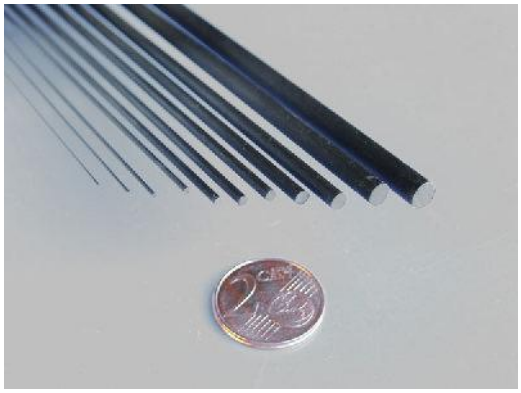

Figure 2. Various diameters round carbon pultruded rods

These designs include diagonal array, tetrahedral, pyramidal, and Kagome lattice truss structures. These designs are shown in Figure 3. The specific properties of TCS panels that are under investigation are the acoustic transmission loss properties, mechanical properties, and the vibration responses of these structures. In order to explore how the structural-acoustic

performance of TCS structure can be controlled and optimized, TCS structure design parameters will be varied so that their effects can be determined. These design variations will be examined in detail in this research.

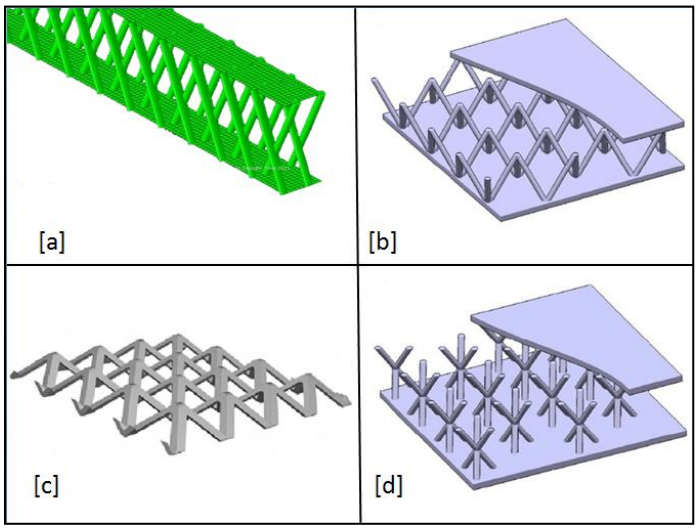

Figure 3. Various TCS core unit cell designs – (a) diagonal array, (b) tetrahedral lattice [20], (c) pyramidal lattice [16], (d) Kagome lattice [20]

1.3 Literature Review

1.3.1 Truss-Core Sandwich Structure Unit Cell Designs

The tetrahedral unit cell design for TCS structure was investigated by a number of researchers [11-13]. Deshpande and Fleck [12] have investigated the elastic properties, yield surface of the homogenized material, and the collapse mechanism of the sandwich panels with one layer of tetrahedral unit cell core. Wicks and Hutchinson [14-15] have estimated the strength of sandwich panels subject to competing failure mechanisms. In addition, they also addressed the optimization of sandwich panels subjected to crushing stress, bending, and transverse shear stress. For the pyramidal unit cell design, Bart-Smith et al [16] used an experimental and analytical approach to examine the in-plane compressive response of pyramidal truss core sandwich columns and identified the various failure mechanisms of such design. For Kagome unit cell design, Hyun et al [17-18] have shown that the isotropy and stability associated with the plastic deformation of Kagome truss core are superior to those of octet truss in terms of

compression and shear loading. Similar benefits were identified by Wang et al [19] through experimental techniques for the Kagome unit cell design.

1.3.2 Vibro-Acoustics Properties of Various Sandwich Panel Designs

The vibration characteristics and the frequency response of TCS structures need to be investigated and compared to provide a basis to design a TCS structure for reduction of cabin noise level. As early as 1959, Kurtze and Watters [21] studied sandwich structures for increasing the acoustic sound TL between adjoining spaces. By investigating the relationship of bending and shear waves to the TL properties of the structure, they suggested that the coincidence frequency can be increased by using a soft core. Lang and Dym [22] created a methodology to design a sandwich panel using only the density and thickness of the core and the face-sheets as design parameters. Their results indicated that there are two fundamental means for improving the TL of sandwich panels. The first is by using the mass law, which states that the more massive and less stiff the panel is, the higher the TL would be. The second is by increasing the core stiffness in order to increase the symmetric coincidence frequency, while maintaining the anti-symmetric coincidence at low frequencies. In terms of aerospace applications of sandwich material, Barton and Mixson [23] and Grosveld and Mixson [24] investigated the possibility of using honeycomb core panel to achieve high TL to attenuate the propeller noise in an aircraft. Moore and Lyon [25] developed a number of analytical models to predict the TL properties of sandwich structures with isotropic and orthotropic core. It was found that coincidence occurs near the conventional double-wall resonance frequency, which can be determined by the stiffness of the core and the mass of the face-sheets, for symmetric modes. However, for a core structure that is orthotropic, the acoustic behaviour depended on the direction of propagation over the surface of the panel. Thamburaj and Sun [26] demonstrated that an anisotropic core can achieve higher TL and further improvement can be attained by proper face-sheet design. El-Raheb [27] studied the frequency response of a two-dimensional truss-like periodic panel using the transfer matrix method. In his research, the effects of panel curvature, sag of cell diagonal member, adding mass to the cell by filling them with water, and damping characteristics were studied. It was found that the structure's vibration and acoustic isolation capabilities strongly strongly depend on the core configuration. This characteristic was also agreed by Ruzzene et al [28] in their study. In addition, El-Raheb and Wagner [29] investigated the sound transmission across a panel structure in contact with an acoustic fluid on

both its surfaces. The TL properties of two different geometries were computed and compared with measurements in his study. Spadoni and Ruzzene [30] found that efficient attenuation can be obtained by confining the deformations to the core element. As a result, varying the design of the unit cell at the core potentially allows tuning the core configuration in order to achieve a specific level of sound attenuation over a specific range of frequency bands. One of the advantages of TCS structure is its potential for optimization due to the variation in unit cell designs and distribution of these designs. A number of researchers have shown that structural acoustic optimization can efficiently mitigate cabin noise. The work of Crane et al. [31] and Cunefare et al. [32] indicated that spatial variations of the design parameters would provide improved TL properties compared to uniform properties. In addition, spatial orientation and directionality must also be considered in order to produce optimal designs. Although there are many papers that discuss the various aspects of different TCS structures, there are none on analyzing a wide range of composite-base TCS designs and how the various design parameters affect these structures in terms of their vibro-acoustic performance. The present research will fill this gap.

1.4 Scope and Thesis Outline

The main goals of this research are to develop methodologies and provide guidelines for designing a TCS structure for reduction of aircraft cabin noise. In order to achieve these objectives, the fundamental nature of the acoustic disturbance must be identified, the process of sound transmission and sound radiation through a partition must be recognized, the wave propagation and vibration nature of the TCS panel must be studied, and the frequency response of the panel upon excitation must be analyzed. Due to the complex nature of the problem and the structure, a mixture of analytical, numerical, and experimental approaches will be used. In Chapter Two, the theoretical background regarding acoustic wave propagation, transmission and radiation will be presented. Understanding the basic mechanics of acoustic noise propagation, it will be shown that the sound radiation performance of a panel structure is closely related to the vibration behaviour of the panel, thus the vibration characteristics of a panel will also be discussed in Chapter Two. Having developed the necessary theoretical analyses of the problem, the detailed analysis of various TCS structures and their results will be presented in Chapter Three. Although a theoretical approach was used to determine the response of beam structures

under force vibration, the TCS beam structures are too complicated to be accurately analyzed by the analytical approach. For this reason, finite element analysis (FEA) will be used to determine the frequency response of TCS beam structures having various core unit cell designs. Parametric studies will be performed using the data obtained from the FEA, and thus design guidelines of TCS structures can be quantitatively determined. The results of the FEA will be presented in Chapter Three. The experimental approach used to determine the TL performance of TCS panels will be described in Chapter Four. The fabrication methods of the TCS panel structure specimen will be explained and illustrated. In addition, the results of the TL window testing of the TCS panels at the Bombardier Aerospace's acoustic chamber facility will also be presented.

Chapter 2

Approach and Analysis

The purpose of this research is to develop the necessary analytical tools, methodologies, and guidelines to design a TCS panel for structural-acoustic performance to reduce cabin noise level. The knowledge of how a fluid exerts forces on a vibrating structure, the vibro-acoustic behaviour of the structure, and sound radiation by the vibrating structures is crucial in the analysis of a TCS panel. For these reasons, the mechanisms that are related to sound transmission, radiation, and response will be discussed in this chapter. Various approaches will be used in this research, which include theoretical analysis, numerical modeling using finite element analysis (FEA), and experimentation, in order to take advantage of the strengths and to overcome the shortfalls of these analysis methods. These methods will be examined in this chapter. Although the absolute sound intensity level and the transmission loss index can be determined, determining the *relative* acoustic and vibrational performance of the TCS structure designs is sufficient to achieve the objectives of this research. Idealization and simplification of the analysis will be made in order to improve the efficiency of this research without sacrificing the validity of its results; these will be discussed in this chapter.

2.1 Transmission and Radiation of Acoustic Noise

As discussed in the previous chapter, the acoustic noise inside a jet powered aircraft cabin is mainly induced by the TBL pressure fluctuation. The TBL excites the exterior of the fuselage, causing it to vibrate and radiate sound into the interior of an aircraft. The radiated sound from the fuselage creates a second pressure field, which excites the structural panels that are enclosing the passenger cabin and the cockpit. The vibration of these structural panels causes cabin air to accelerate, which is in contact with the surface, changing the density of the fluid, and thus producing noise. In order to analyse the acoustic performance of these structural panels, it is

beneficial to understand the mechanisms and mathematical models of these sound transmission processes.

2.1.1 Turbulent Boundary Layer Pressure Fluctuation Loading on Fuselage

Due to the random nature of TBL excitation, the resultant pressure fluctuation on the fuselage can be described by statistical analysis, which is usually known as the pressure power spectral density (PPSD). Assuming a fully developed flow and zero mean pressure gradient, the flow can be considered to be stationary and homogeneous in space. Let the flow be in the x-direction along the fuselage, and the lateral direction is in the y-direction, which is perpendicular to the x-axis and on the surface of the fuselage, then the PPSD over a surface at a location x and y can be defined as:

$$S(x, \xi_x, \xi_y, \omega) = \langle P_{ref}(x_{ref}, y_{ref}, \omega), P(x, y, \omega) \rangle, \tag{2.1}$$

where P_{ref} is the reference pressure at the reference location x_{ref} and y_{ref}, and P is the pressure on a fuselage panel located at x and y. Using Corcos' formulation [33, 34], the PPSD can be approximated by:

$$S(x, \xi_x, \xi_y, \omega) = S_{ref}(x, \omega) e^{-\frac{\alpha_x \omega |\xi_x|}{U_c}} e^{-\frac{\alpha_y \omega |\xi_y|}{U_c}} e^{-\frac{i\omega |\xi_x|}{U_c}}, \tag{2.2}$$

where α_x and α_y are empirical parameters, which represent the loss of coherence in the longitudinal and transverse directions, ω is the angular frequency, and U_c is the convective speed of the TBL. The reference PPSD, $S_{ref}(x, \omega)$, can be estimated by Efimtsov model [35]:

$$S_{ref}(x, \omega) = \frac{\tau_W^2(x)\delta(x)}{U_\tau(x)} \frac{0.01\pi}{1 + 0.02Sh^{2/3}(x, \omega)}, \tag{2.3}$$

with:

$$U_\tau(x) = U_\infty \sqrt{\frac{C_f(x)}{2}}, \tag{2.3a}$$

$$\tau_w(x) = \frac{1}{2}\rho U_\infty^2 C_f(x), \tag{2.3b}$$

$$Sh(x,\omega) = \frac{\omega\delta(x)}{U_\tau(x)}, \tag{2.3c}$$

where U_τ is the friction velocity, τ_W is the mean wall shear stress, C_f is the friction coefficient, δ is the boundary layer thickness, Sh is the Strouhal number, and U_∞ is the free stream velocity. In addition, $C_f(x)$ and $\delta(x)$ can be found using semi-empirical expressions for turbulent boundary layers [36, 37]:

$$C_f(x) = 0.37(\log_{10} Re_x)^{-2.584}, \tag{2.4a}$$

$$\delta(x) = 0.37 Re_x^{-\frac{1}{5}}\left[1 + \left(\frac{Re_x}{6.9\times 10^7}\right)^2\right]^{\frac{1}{10}}, \tag{2.4b}$$

where Re_x is the streamwise Reynolds number. Using this model to estimate the PPSD of a TBL, the induced exterior pressure can be determined. The structural response of the fuselage to such pressure excitation is in the form of mechanical vibration, which will cause sound radiation and create acoustic noise in an aircraft cabin. Assuming that an aircraft fuselage is made up of a finite number of individual panels with simply supported boundary conditions, the response of a panel can be determined by the plate governing equation for a untensioned plate (unpressurized cabin) and a tensioned plate (pressurized cabin) respectively by [38]:

$$D_p\nabla^4 w + \rho_P h_p \ddot{w} + \zeta_p \dot{w} = P(x,y,t), \tag{2.5a}$$

$$D_p\nabla^4 w + \rho_P h_p \ddot{w} + \zeta_p \dot{w} - \left(T_x f_x^2 + T_y g_y^2\right)w = P(x,y,t), \tag{2.5b}$$

where D_p is the panel stiffness constant, $w(x,y,t)$ is the panel displacement in the normal direction, ρ_P is the density of the panel, h_P is the thickness of the panel, ζ_p is the damping coefficient of the plate, T_x and T_y are the in-plane tensions in the x- and y- directions respectively, f_x and g_y are the vibration mode specific coefficients, and $P(x,y,t)$ is the external pressure. D_p, f_x, and g_y are given by the following formulas respectively:

$$D_p = \frac{E_p h_p^3}{12\left(1-\nu_p^2\right)}, \tag{2.6a}$$

$$f_x = \frac{m_x \pi}{a}, \tag{2.6b}$$

$$g_y = \frac{m_y \pi}{b}, \tag{2.6c}$$

where E_p is the elastic modulus of the plate, ν_p is the Poisson's ratio, a and b are the length and width of the plate respectively, and m_x and m_y are the plate modes number in the *x*- and *y*-direction of the plate. It is assumed that the fuselage panel is thin compared to its other dimensions, therefore shear deformation and rotary inertia can be neglected in the formulations at this point. In order to determine the displacement of a plate, $w(x,y,t)$, the response of a structure can be modelled in terms of a modal expansion such that at each excitation frequency, the response is determined by a summation of modal terms [38]:

$$w(x,y,t) = \sum_{m_x=1}^{M_x} \sum_{m_y=1}^{M_y} A_{m_x}(x) B_{m_y}(y) q(t)\,, \tag{2.7}$$

where $A_{m_x}(x)$ and $B_{m_y}(y)$ are the normal modes of the plate, which define the spatial variation of the deflection $w(x,y,t)$, $q(t)$ is the temporal variation of $w(x,y,t)$, and M_x and M_y are the number of plate modes in the *x*- and *y*- directions, respectively, therefore $M = M_x \times M_y$ is the total number of plates modes being considered in the analysis. The normal modes for a plate can be represented by the following functions:

$$A_{m_x}(x) = \sqrt{\frac{2}{a}} \sin\left(\frac{m_x \pi x}{a}\right), \tag{2.8a}$$

$$B_{m_y}(y) = \sqrt{\frac{2}{b}} \sin\left(\frac{m_y \pi y}{b}\right). \tag{2.8b}$$

The corresponding natural frequencies with the aforementioned idealization and boundary conditions for an unpressurized and pressurized cabin are respectively:

$$\omega_p = \sqrt{\frac{D_p}{\rho_p h_p}}\left[\left(\frac{m_x \pi}{a}\right)^2 + \left(\frac{m_y \pi}{b}\right)^2\right], \tag{2.9a}$$

$$\omega_p = \sqrt{\frac{1}{\rho_p h_p}}\left[D_p\left(f_x^2 + g_y^2\right)^2 + T_x f_x^2 + T_y g_y^2\right]. \tag{2.9b}$$

Idealizing the curved fuselage shells by flat plates can reduce the complexity of the problem while providing a good estimate to the sound radiated by the panels. However, it should be noted that there are a number of drawbacks associated with such assumptions. For example, the effect on the flexural wave dispersion characteristics of a curved panel cannot be represented by the above formulations due to the flat plate assumptions. The curvature associated with a curved panel allows coupling of forces in the radial and tangential directions when the shell is stressed. One of the implications of this effect is the increase of radiation efficiency of the curved panel because the flexural wave phase velocities increases if the frequency is below the ring frequency. This effect diminishes as the radius of a fuselage increases. Due to the large radius of an aircraft, the flat plate assumption is valid and will reduce the complexity of the analysis. It is rather difficult to solve for the vertical deflection $w(x, y, t)$, which is needed to determine the sound radiation by the fuselage. However, the purpose of the current research is to determine the acoustic performance of the interior TCS panel, which encloses the cabin, therefore certain idealizations and simplifications can be made in order to perform the research more efficiently. This will be explained in more detail later on in this chapter. In addition, the simply supported boundary conditions are idealized and not representative a of practical aircraft structure. However, Berry et al [39] show that clamping the edges of a panel makes insignificant difference to the modal radiation efficiency, slightly decreasing that of the low order modes and increasing that of higher order modes by a maximum factor of 2.5, which is equivalent to 4 dB. For these reasons, a simply supported boundary condition is a good approximation to the panel's complicated boundary conditions, which are caused by the fact that the panels are dynamically coupled to continuous structures.

2.1.2 Sound Radiation from Fuselage Panels

Assuming that the time and spatial variations of the fuselage panel displacement are known, the next step is to determine the general vibration induced pressure field inside the fuselage, but outside the cabin. The normal vibration velocity distribution of the fuselage panel is $\dot{w}(x,y,t)$ or $v_n(x,y,t)$. Using the integral formulation derived by Lord Rayleigh:

$$P(\boldsymbol{r},t) = \frac{j\omega\rho_0}{2\pi} e^{j\omega t} \int_S \frac{\tilde{v}_n(\boldsymbol{r}_s) e^{-jkR}}{R} dS, \tag{2.10}$$

and a modal representation of the velocity distribution (neglecting the temporal variation):

$$\tilde{v}_n(x,y) = \tilde{v}_{m_x m_y} \sin\left(\frac{m_x \pi x}{a}\right) \sin\left(\frac{m_y \pi y}{b}\right), \tag{2.11}$$

where ρ_0 is the density of the medium, $\boldsymbol{r}_s$ is the position vector of the observation point from a elemental surface δS having normal velocity amplitude $\tilde{v}_n$, R is the magnitude of the position vector $\boldsymbol{r}_s$, and $\tilde{v}_{m_x m_y}$ is the magnitude of the modal specific velocity. The reason that a modal specific quantity is used is because sound radiation from lightly damped panels can only radiate efficiently at their natural frequency or at their discrete natural modes, which causes resonant vibration. In contrast to the previous section, a complex exponential mathematical representation was used to describe quantities that vary in time and space, which are fundamental to the nature of wave motion in general. Using this kind of representation, simple harmonic variations in time can be conveniently described. For example, a quantity that varies with time:

$$g(t) = G\cos(\omega t + \phi), \tag{2.12}$$

where G symbolises amplitude and ϕ is the phase. This quantity can also be represented by:

$$g(t) = Re\{\tilde{F} e^{jwt}\}, \tag{2.13}$$

and

$$\tilde{F} = G e^{j\phi}. \tag{2.14}$$

Using the modal specific velocity and Rayleigh integral formulation, the radiated pressure variation at location [*x,y,z*] is [40]:

$$P(x,y,z,t) = \frac{j\omega\rho_0\tilde{v}_{m_x m_y}e^{j\omega t}}{2\pi}\int_0^a\int_0^b \frac{\sin\left(\frac{m_x\pi x}{a}\right)\sin\left(\frac{m_y\pi y}{b}\right)e^{-jkR}}{R}dxdz. \quad (2.15)$$

However, in order to solve analytically for the pressure field efficiently, a cylindrical coordinate system is used, and the formulation becomes:

$$P(r,\theta,\gamma,t) = \frac{j\omega\rho_0\tilde{v}_{m_x m_y}e^{-jkr}e^{j\omega t}}{2\pi r}\int_0^a\int_0^b \sin\left(\frac{m_x\pi x}{a}\right)\sin\left(\frac{m_y\pi y}{b}\right)e^{\left[j\left(\frac{\alpha x}{a}\right)+j\left(\frac{\beta z}{b}\right)\right]}dxdz, \quad (2.16)$$

where

$$\alpha = ka\sin\theta\cos\gamma\,, \quad \beta = kb\sin\theta\cos\gamma\,, \quad (2.16a, 2.16b)$$

and k is the wavenumber. The analytical solution of the pressure field was determined by Wallace [41]:

$$P(r,\theta,\gamma,t) = j\tilde{v}_{m_x m_y}k\rho_0 c\frac{e^{-jkr}}{2\pi r}\frac{ab}{m_x m_y\pi^2}\left[\frac{(-1)^{m_x}e^{-j\alpha}-1}{\left(\alpha/m_x\pi\right)^2-1}\right]\left[\frac{(-1)^{m_y}e^{-j\beta}-1}{\left(\beta/m_y\pi\right)^2-1}\right], \quad (2.17)$$

where c is the sound speed in the medium.

2.1.3 Transmission and Radiation of Acoustic Noise into the Cabin

Now that the radiated pressure field inside of a fuselage is determined, the fluid loading on the cabin structures, such as the floor panels and the wall enclosures, can be resolved. Assuming that the cabin is made up of array of individual panels, the resultant displacement or the vibration characteristic is represented by $w_c(x,y,t)$. The fluid-structure interaction between the cabin panels and the air between the fuselage and the cabin enclosures can be considered to be passive in the sense that the small-amplitude motion of the vibration cabin panels does not significantly

alter the exciting force. Although fluid loading can be influenced by reflection of radiated sound from the enclosure and fuselage interior boundaries, it will be assumed that its effect is insignificant at this stage of the research. Under these conditions, the sound transmission through the cabin enclosures can be idealized as a forced vibration problem on a plate with simply supported boundary conditions on all sides. Using a forced vibration analysis, the displacement, $w_c(x,y,t)$, as well as the surface panel velocity, $v_c(x,y,t)$, can be found, which can be used to determine the acoustic noise level inside the cabin by using the methods shown in the previous section. In addition, the sound intensity level is an important indicator for the acoustic noise level in the cabin and it can be determined by the following relationship [40]:

$$\bar{I}(r,\theta,\vartheta) = 2\rho_0 c \left|\tilde{v}_{m_x m_y}\right|^2 \left(\frac{kab}{\pi^3 r m_x m_y}\right)^2 \left\{\frac{\cos\left(\frac{\alpha}{2}\right)\cos\left(\frac{\beta}{2}\right)}{[(\alpha/m_x\pi)^2-1]\left[\left(\beta/m_y\pi\right)^2-1\right]}\right\}^2 . \tag{2.18}$$

It can be observed that both the radiated pressure field and sound intensity formulations have a direct relationship with the modal velocity, which is directly related to the normal panel surface velocity according to Equation [2.10]. For these reasons, the velocity data computed from a forced vibration analysis on the cabin panels will be sufficient to determine which cabin panel designs will provide a lower sound intensity in the cabin, as well as higher transmission loss properties. Using a forced vibration analysis instead of a coupled structural-acoustic analysis to determine which TCS structure design is more suitable for cabin panel sound insulation can greatly improve the research efficiency, enabling a focus on determining how to control the structural acoustic performance of TCS structure designs. It should be emphasised that the goal of this research is not to determine the absolute acoustic performance of a TCS panel, but to determine the relative performance between various TCS structure designs so that the proper design selection and approach can be identified. For these reasons, there is an opportunity to improve the research efficiency even further by performing a forced vibration analysis on a beam structure instead of a plate structure so that the analysis can be computationally efficient and the closed-form analytical solution can be obtained in a relatively straightforward approach. A beam is a one dimensional elastic system with only one independent spatial variable, which is the length along the member. However, a TCS panel or plate is a two dimensional elastic system

with two independent spatial variables, the length and the width. Although a beam has one fewer independent spatial variable, the restoring forces in both systems arise from in-plane tensile or stretching forces, and bending moment and transverse shear forces are active. For these reasons, the basic kinematics of the classical theory of thin plates is the same as that of Euler-Bernoulli beams. The governing equations for thin uniform beam and plate can be represented by the following two inhomogeneous partial differential equations respectively:

$$EI_b \frac{\partial^4 w}{\partial x^4} + \rho A \frac{\partial^2 w}{\partial t^2} = q(x,t), \tag{2.19}$$

$$EI_p \nabla^4 w + \rho h \frac{\partial^2 w}{\partial t^2} = q(x,y,t), \tag{2.20}$$

where I_b is the moment of inertia of the beam, which depends on the shape of the beam's cross section, A is the cross-sectional area of the beam, $q(x,t)$ or $q(x,y,t)$ is the applied forced, I_p is equal to $h^3/12(1-v^2)$, h is the thickness of the plate, and ∇^4 is the biharmonic operator. For thicker beams, the effect of shear deformation and rotary inertia can be incorporated into the formulations in the same manner as in a thick plate. In addition, for a plate which has simply supported boundary condition, if the phase coincidence is satisfied independently in the two orthogonal directions, *x* and *y*, then it is satisfied everywhere. The wavenumber vector components in these directions at the natural frequencies correspond to those for a similar beam of equal length. For these reasons and the purpose of the research, the analysis of forced vibration of a beam can provide much insight into the structural-acoustic characteristics of a TCS panel, and provide us the information to tailor the acoustic properties of TCS panels.

2.2 Forced Vibration Analysis of a TCS Beam

By theoretically evaluating the mechanical response of a beam with a simply supported boundary condition under a normally incident, time-varying pressure load, the beam's surface acoustic pressure gradient can be determined using the normal surface velocity through the Rayleigh integral as shown in Equation [2.11], which can be used to evaluate the induced pressure field and the sound radiation intensity. Therefore by comparing the normal surface velocity of the TCS beam structures with different core and face-sheet designs, the acoustic performance of the TCS structure design can be evaluated and the response characteristics of the various structural

design parameters can be identified. In addition, at low frequency excitation, a TCS beam will behave like a uniform beam and the response will only depend on the beam's overall elastic modulus, cross-sectional area, moment of inertia, density, and the shear modulus. At higher frequency excitation, the transverse wave propagation is controlled by the core shear stiffness and by the individual faceplate-bending stiffnesses [21]. Therefore a numerical approach, such as finite element analysis, is required to provide sufficient detail in the analysis. However, knowledge of a uniform beam's vibration response will provide much insight for the design of TCS structures since the most important frequency range for aircraft cabin design is below 2000 Hz. For these reasons, the goal of this section is to develop the formulations to determine the normal surface velocity of a uniform beam under a normally incident pressure load with a simply supported boundary condition.

2.2.1 Governing Equations of a Beam

The governing equation of a uniform beam developed by the classical beam theory is illustrated in Equation [2.19]. Although the beam's surface deflection and velocity can be evaluated using this formulation, the effect of the shear modulus on the response of the beam is absent , which is important for the analysis of sandwich structure and response of a structure at high frequency excitation. In addition, classical Euler-Bernoulli beam theory assumes that the plane cross-sections remain planar after deformation, which implies that shear deformation is neglected. This assumption is valid for thin plates such as the fuselage panel, but for thicker plates such as the TCS panel, this assumption will introduce error into the results of the response. In addition, using the Euler-Bernoulli beam theory, the phase velocity of the propagating wave increases without limit for increasing wavenumber [42]:

$$c = \pm\sqrt{\frac{EI}{\rho A}}k, \tag{2.21}$$

where k is the wavenumber and c is the phase velocity. This prediction of infinite phase velocity is non-physical and it is due to neglect of rotary inertia and shear deformation. For these reasons, the formulation required to model correctly the behaviour of TCS beam structure must include shear deformation and rotary inertia. Using Timoshenko beam theory, both the shear deformation and rotary inertia effect can be included, and it is illustrated here to provide insight

into the design of a TCS structure. Taking into account of both the bending, ψ, and the shear effect, γ_0, the slope of the deformation is:

$$\frac{\partial w}{\partial x} = \psi + \gamma_0. \tag{2.22}$$

The relationship between bending moment and the curvature is:

$$\frac{M}{EI} = -\frac{\partial \psi}{\partial x}. \tag{2.23}$$

For the shear component, Timoshenko showed that the shear force is related to the shear stress τ, shear strain γ, and shear strain at the centroidal axis γ_0 according to the following formulae respectively:

$$V = \int \tau dA = G \int \gamma dA = (G\gamma_0 A)\kappa\,, \tag{2.24}$$

where κ is the Timoshenko shear coefficient, which depend on the shape of the cross-section of the beam. Using the Equation [2.22] and [2.24], the shear stress can be expressed as:

$$V = AG\kappa\left(\frac{\partial w}{\partial x} - \psi\right). \tag{2.25}$$

By summing the forces in the vertical direction, the equation of motion can be obtained:

$$\frac{\partial V}{\partial x} + q = \rho A \frac{\partial^2 w}{\partial t^2}. \tag{2.26}$$

By summing the moment, another equation of motion is found:

$$V - \frac{\partial M}{\partial x} = \rho I \frac{\partial^2 \psi}{\partial t^2}. \tag{2.27}$$

Substituting the expression for bending moment and shear force into the two governing equations [2.26] and [2.27] gives the following governing equations for the Timoshenko beam theory:

$$GA\kappa\left(\frac{\partial\psi}{\partial x}-\frac{\partial^2 w}{\partial x^2}\right)+\rho A\frac{\partial^2 w}{\partial t^2}=q(x,t), \tag{2.28}$$

$$GA\kappa\left(\frac{\partial w}{\partial x}-\psi\right)+EI\left(\frac{\partial^2\psi}{\partial x^2}\right)=\rho I\frac{\partial^2\psi}{\partial t^2}. \tag{2.29}$$

In order to determine the normal surface velocity of a specific beam structure, one must solve these coupled, inhomogeneous partial differential equations. In addition to determining the normal surface velocity, another quantity is also important for evaluating the acoustic or vibration characteristics of the beam structure, which is the natural frequency of the beam. Natural frequency is a free vibration phenomenon, while resonance is associated with forced vibration. When a structure vibrates at its natural frequencies or eigenvalues, large amplitude response to the excitation is induced, and the structure can radiate sound at its maximum efficiency. The knowledge of the natural frequencies can provide essential information regarding the acoustic behaviour of the structure, and therefore the natural frequencies of a general beam structure will be explored first. Using equation [2.28] to solve for $\partial\psi/\partial x$, substituting the result into equation [2.29], and setting $q(x,t)=0$ for this free vibration analysis, the equation of motion for the free vibration of a uniform beam is:

$$EI\frac{\partial^4 w}{\partial x^4}+\rho A\frac{\partial^2 w}{\partial t^2}-\rho I\left(1+\frac{E}{\kappa G}\right)\frac{\partial^4 w}{\partial x^2\partial t^2}+\frac{\rho^2 I}{\kappa G}\frac{\partial^4 w}{\partial t^4}=0, \tag{2.30}$$

Define $\epsilon^2=EI/\rho A$ and $r^2=I/A$, and the previous equation becomes:

$$\varepsilon^2\frac{\partial^4 w}{\partial x^4}+\frac{\partial^2 w}{\partial t^2}-r^2\left(1+\frac{E}{\kappa G}\right)\frac{\partial^4 w}{\partial x^2\partial t^2}+\frac{\rho r^2}{\kappa G}\frac{\partial^4 w}{\partial t^4}=0. \tag{2.31}$$

Assuming that the solution for $w(x,t)$ has the form:

$$w(x,t)=\sin\left(\frac{n\pi x}{l}\right)\cos(\omega_n t), \tag{2.32}$$

where *n* is the number of the natural mode, l is the length of the beam, and ω_n is the n^{th} natural frequency of the system. Substituting equation [2.32] into [2.31], the frequency equation of the beam structure is:

$$\omega_n^4\left(\frac{\rho r^2}{\kappa G}\right)-\omega_n^2\left(1+\frac{n^2\pi^2r^2}{l^2}+\frac{n^2\pi^2r^2}{l^2}\frac{E}{\kappa G}\right)+\left(\frac{\varepsilon^2n^4\pi^4}{l^4}\right)=0. \tag{2.33}$$

The solution of the frequency equation of a general beam can be found by using the quadratic formula, and therefore the expression for the natural frequency is:

$$\omega_n^2=\frac{\left(1+\frac{n^2\pi^2r^2}{l^2}+\frac{n^2\pi^2r^2}{l^2}\frac{E}{\kappa G}\right)\pm\sqrt{\left(1+\frac{n^2\pi^2r^2}{l^2}+\frac{n^2\pi^2r^2}{l^2}\frac{E}{\kappa G}\right)^2-4\left(\frac{\rho r^2}{\kappa G}\right)\left(\frac{\epsilon^2n^4\pi^4}{l^4}\right)}}{2\left(\frac{\rho r^2}{\kappa G}\right)}. \tag{2.34}$$

If the effect of rotary inertia alone is considered (Rayleigh beam theory), the shear coefficient κ can be set to 0 in the equation of motion for the beam, and the frequency equation is reduced to:

$$\omega_n^2=\frac{\epsilon^2n^4\pi^4}{l^4\left(1+\frac{n^2\pi^2r^2}{l^2}\right)}. \tag{2.35}$$

If the effect of shear deformation alone is considered, the term $\rho I(\partial^2\psi/\partial t^2)$ can be set to 0 in the equation of motion for the beam, and the frequency equation is reduced to:

$$\omega_n^2=\frac{\epsilon^2n^4\pi^4}{l^4\left(1+\frac{n^2\pi^2r^2}{l^2}\right)\frac{E}{\kappa G}}. \tag{2.36}$$

If both the effect of rotary inertia and shear deformation are neglected in the formulation, equation [2.31] becomes the classical Euler-Bernoulli beam theory, which gives the natural frequency of:

$$\omega_n^2=\frac{\epsilon^2n^4\pi^4}{l^4}. \tag{2.37}$$

By comparing the natural frequencies obtained by the four theories for a typical beam with a simply supported boundary condition, the result is shown in Figure 4. It can be seen that the four theories are in close agreement to each other at low natural frequencies or mode numbers, and

they diverge from each other as the natural frequencies are increased. At the 10th mode, there is a 7.5% difference between the natural frequency predicted by the Timoshenko beam theory and the Euler-Bernoulli beam theory. Using the solution from the Timoshenko beam theory, one can accurately predict the natural frequency of a uniform beam with a simply supported boundary condition. In terms of forced vibration, if there is a coincidence between the excitation frequency and the natural frequency, resonance occurs. Knowing the excitation frequency, one can design a beam to avoid coincidence, thus high level of sound radiation can be avoided.

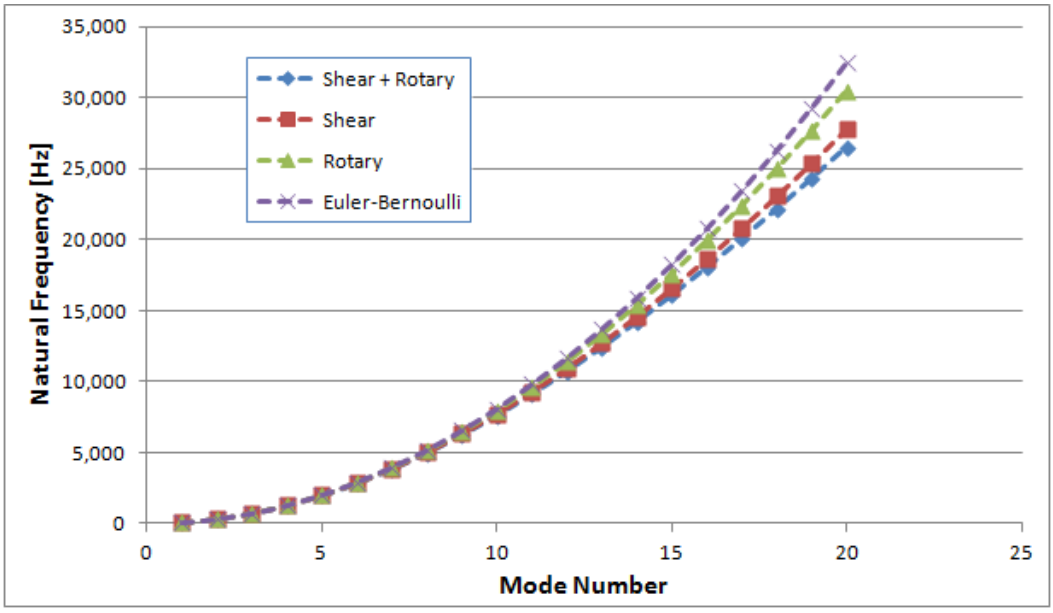

Figure 4. Natural frequencies from four different beam theories – Euler-Bernoulli, rotary-inertia only, shear deformation only, and Timoshenko beam theory

In order to determine the response of a beam across a wide spectrum of frequencies, the displacement and the velocity time history must be determined. The method of separation of variables and normal mode expansion can be used to determine the beam's response. It is assumed that the beam's response, $w(x,t)$, can be presented in the form of a product of a function dependent on the spatial coordinate x and a function dependent on time t, therefore it can be represented by:

$$w(x,t) = \sum_{n=1}^{\infty} Y_n(x)T_n(t), \tag{2.38}$$

where $Y_n(x)$ are the normal modes or the eigenfunctions of the system and $T_n(t)$ represents the temporal variation of $w(x,t)$. Substituting the assumed solution to $w(x,t)$ (Eqn [2.38]) to equation [2.31], and applying the boundary conditions to the system, the solution of the normal mode for a simply support beam, $Y_n(x)$, can be expressed in the following general form:

$$Y_n(x) = \sin\frac{n\pi x}{l}. \tag{2.39}$$

The next step is to determine the time function $T_n(t)$ in order to determine the time variation forced response of the system. Using the Duhamel integral, $T_n(t)$ has the following general expression:

$$T_n(t) = M_n \cos\omega_n t + N_n \sin\omega_n t + \frac{1}{\rho A \varphi \omega_n}\int_0^t Q_n(t') \sin\omega_n(t-t')dt', \tag{2.40}$$

where the first two terms on the right-hand side represent the transient response, and the third term denotes the steady state response resulting from the forcing function. The variable φ is given by:

$$\varphi = \int_0^l Y_n^2(x)dx, \tag{2.41}$$

and the generalized force corresponding to $T_n(t)$ is:

$$Q_n(t) = \int_0^l q(x,t)\, Y_n(x)dx. \tag{2.42}$$

Let the excitation force be a single-frequency harmonic load with a unit magnitude, therefore:

$$q(x,t) = \sin\omega t, \tag{2.43}$$

then $Q_n(t)$ becomes:

$$Q_n(t) = \int_0^l \sin(\omega t)\sin\left(\frac{n\pi x}{l}\right)dx = \frac{l}{n\pi}\sin(\omega t)[1-\cos(n\pi)]. \tag{2.44}$$

For the symmetric modes, where *n* is an odd number:

$$Q_n(t) = \frac{2l}{n\pi}\sin(\omega t), \tag{2.45}$$

and for the antisymmetric modes, where *n* is an even number, $Q_n(t)$ is equal to zero. Substitute the value of $Q_n(t)$ into the steady state part of equation [2.40] and ignore the transient part:

$$T_n(t) = \frac{4}{\rho A n\pi}\frac{\sin(\omega t)}{\omega_n^2 - \omega^2}, \tag{2.46}$$

where the value φ was calculated to be:

$$\varphi = \int_0^l Y_n^2(x)dx = \int_0^l \sin^2\left(\frac{n\pi x}{l}\right)dx = \frac{l}{2}. \tag{2.47}$$

Substitute the value of $T_n(t)$ and $Y_n(x)$ into equation [2.38], the beam's response can be found in a modal summation format:

$$w(x,t) = \frac{4}{\rho A\pi}\sum_{n=1}^{\infty}\frac{1}{n(\omega_n^2 - \omega^2)}\sin\left(\frac{n\pi x}{l}\right)\sin(\omega t)\,. \tag{2.48}$$

A typical response of a uniform beam with a simply supported boundary condition (translational motions are fixed at both ends, while rotation is allowed) is shown in Figure 5. The response is measured by the root mean squared (RMS) velocity of the beam, which can be obtained by integrating the result given by equation [2.48]. The normal incident pressure load is applied on the top surface and the RMS velocity is measured on the bottom surface. RMS velocity is an indicator of the kinetic energy of the transverse motion of the beam and it is directly proportional to the radiated sound intensity [43]. The definition for RMS velocity is:

$$V_{RMS} = \sqrt{\frac{1}{m}\sum_{k=1}^{m}\dot{w}_k^2}\,, \tag{2.49}$$

where *k* represents the spatial location where the velocity is measured and *m* is the total number of data points. Using this method of analyzing a TCS beam, the response of a beam is idealized by an equivalent homogeneous beam whose properties can be determined through the application

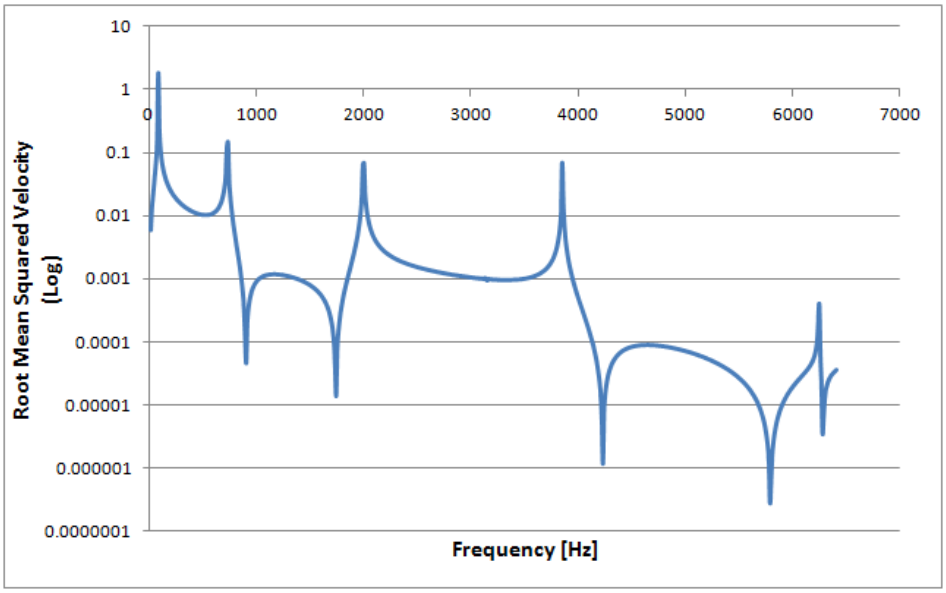

Figure 5. Root-mean-squared velocity response of a Timoshenko beam with simply supported boundary condition (measured at center point)

of basic structural mechanics at the low-frequency range. However, when the wavelengths of vibration are similar to the length of the core trusses, homogenization fails, and a more detailed analysis is required to depict accurately the characteristics of a beam under a harmonic pressure load. Finite element analysis (FEA) is used for this purpose and it will be discussed in the following section.

2.3 Finite Element Analysis

Due to the nature of the problem, an explicit non-linear FEA code, ABAQUS, is used for the vibration analyses in this research. As discussed in Section *2.1.3*, a TCS beam structure will be analyzed using FEA instead of a plate structure. The reason for this is because the required simulation run-time for a complete computational model of a TCS panel structure is excessive for this developmental effort. A panel model will require at least 600,000 elements, and a typical frequency response curve for a single TCS structure design will take 200 simulation runs. For this reason, TCS beam structure models were used to determine the trend of their vibro-acoustic behaviours, and to develop design guidelines for TCS panel structures. The face-sheets are modeled by shell elements and the trusses are modeled by beam elements, both using reduced integration in order to improve computational efficiency by reducing the numerical timestep and

avoiding non-physical high stiffness behaviour, such as shear locking. Since under integrated elements may suffer from hourglassing, which is zero energy deformation mode, hourglass modes will be suppressed using mesh refinement techniques and applying nodal hourglass restoring forces. The hourglass energy will be monitored in order to reduce non-physical behaviour. Adequate number of integration points through the thickness of an element is needed in order to prevent plastic hinge behaviour. A study period should be chosen to accommodate the lowest frequency vibration. The timestep will be determined by the smallest element in the discretized model, and the sampling interval should be set to equal to the Nyquist distance times a safety factor of 0.8 to avoid aliasing. The element size should be chosen to represent properly the physical sound speed. Due to the nature of the problem, it is assumed that the deformation of the beam is small, therefore a linear elastic material model is used in the analysis. For a simply supported boundary condition, three principle axes translational degrees of freedom are fixed, and the rotational freedoms in the three principle axes are not restrained. A typical FEA analysis for a TCS beam structure is shown in Figure 6. The details of the various material properties, the

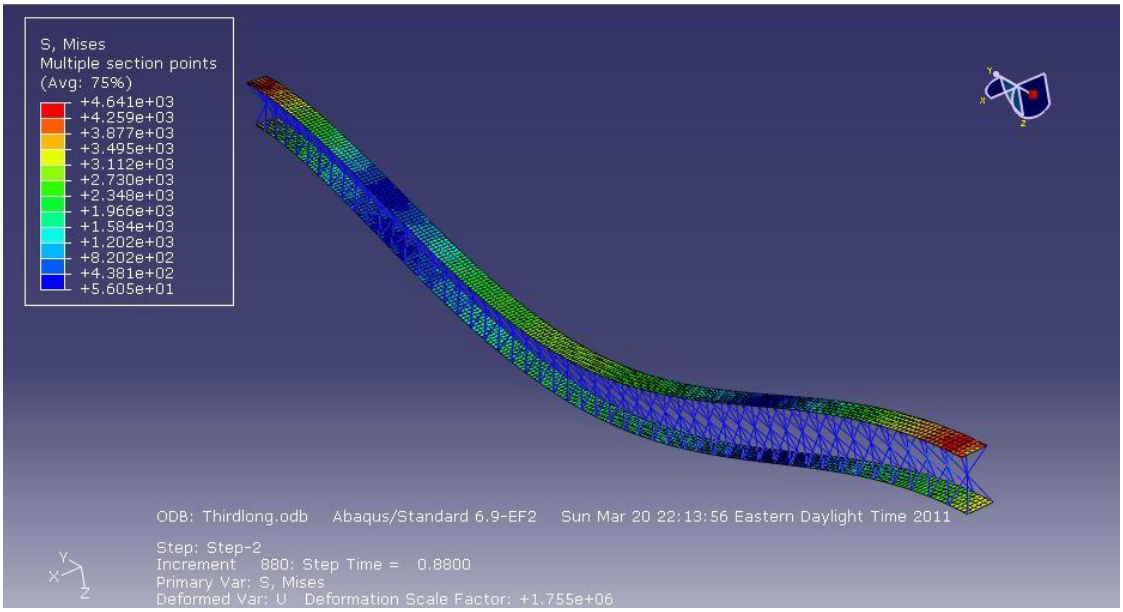

Figure 6. Typical finite element analysis of a TCS beam with a simply supported boundary condition

geometrical attribute of the models, and the various FEA results will be presented in the Chapter Three. Using the results obtained from the analytical approach, as described in Section 2.2, and the results from the FEA, sensitivity studies and parametric studies can be performed. The

results of these studies will identify the characteristics of various design parameters of a TCS structure, hence general design guidelines can be developed, and the methodologies for designing a TCS structure for superior acoustic performance can be formulated.

2.4 Acoustic Chamber Experiments

Although the analytical efficiency was drastically improved by using a beam structure model instead of a plate structure, the actual acoustic performance of an equivalent TCS panel structure is yet to be determined. The TCS panels are fabricated at the Multifunctional Structures Lab at UTIAS using a set of fixtures, which are developed specifically for this research project. An example of a fabrication setup is shown in Figure 7. The designs of these experimental TCS panels are based on the analytical and FEA results. In order to determine the actual performance of a TCS panel, experiments will be carried out. The experimental component of this research

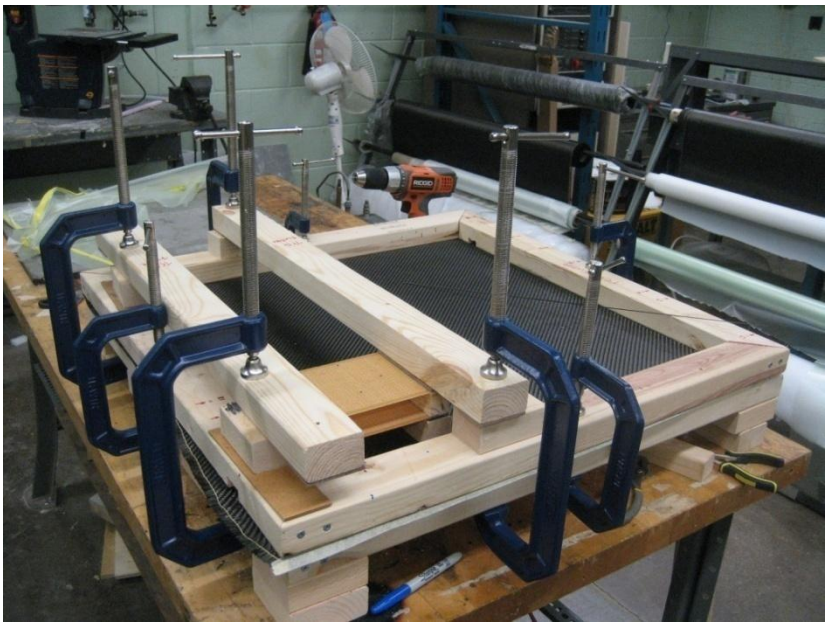

Figure 7. Typical TCS panel fabrication setup using UTIAS Multifunctional Structures Lab fixture design

project is partially funded by an Engage Grant, which provides funding from the Canadian government as well as in-kind support from an industry partner. The industry partner for this grant is Bombardier Aerospace (BA) who provided us with access to their acoustic chamber for acoustic performance testing of the various TCS panel designs. The acoustic chamber is designed to measure the transmission loss (TL) properties of a panel inserted in its TL window.

Random white noise is produced in the chamber and it is measured by three condenser microphones inside the chamber. A sound intensity probe is used to measure the sound intensity level just outside of the TL window, where a TCS panel is installed. The goal of the experiment is to show the difference in acoustic performance by changing the truss core design. The details of the fabrication process, experimental setup, and the testing results will be presented in Chapter Four of this report.

Chapter 3

Results and Discussions

The analysis results obtained using the formulations and the methodologies described in the previous chapters are presented in this section. In addition, the significance of these results regarding their contribution to the objectives of this research project will also be discussed in detail. The results of the theoretical and numerical analyses are presented in this chapter. The results of the experimental part of this research project will be presented in the Chapter Four.

The most important vibro-acoustic characteristics of a TCS structure that affect the radiated noise level inside a cabin include the radiated sound power, radiation efficiency, and resonance frequencies. As discussed in Chapter Two, all these quantities are related to the root-mean-square (RMS) velocity of the surface of an excited structure. By exciting a beam structure using a spectrum of frequencies, and measuring the RMS velocities, a frequency response analysis can be created and used to access the performance of a particular TCS structure design. An example of a typical frequency response analysis is shown in Figure 5 in Chapter Two. A frequency response analysis provides information regarding the magnitude of the response, as well as the resonance frequency of the structure. The latter identifies the excitation frequencies at which the structure radiates sound most efficiently. Using this information, engineers can design the vibro-acoustic characteristic of a structure to avoid coincidence with any of the predominant excitation frequencies and compare the vibro-acoustic performance of various TCS panel designs.

3.1 Analytical Analysis

Using the analytical approach in Chapter Two, the response of a uniform Timoshenko beam structure with simply supported boundaries under a single-frequency harmonic load with a normal incident angle can be represented by Equation [2.48]. Although a TCS structure cannot

strictly be represented by a uniform beam due its inhomogeneous nature, by idealizing the structure as a homogeneous system, one can estimate its low-frequency response as well as to understand the general trend of the performance gradient as the structural parameters changed. In addition, it is assumed that the structural surface density is much higher than the fluid density, and therefore the effect of the medium on the frequency response analysis can be neglected. For these reasons, a frequency response analysis on a uniform beam will be conducted first in this research. Note that damping has been neglected in this idealized model.

3.1.1 Initial Frequency Response Analysis Using Theoretical Formulation

The range of frequency that human can perceive is approximately between 20 Hz to 20 kHz, which has considerable variation between individuals. However, the most important frequencies for cabin noise reduction analysis are from 20 Hz to 4000 Hz; therefore focus will be on analyzing structures in this frequency range. The low-frequency range is between 20 Hz and 2,000 Hz, the mid-frequency range is between 2,000 Hz and 4,000 Hz, and the high-frequency range is between 4,000 Hz and 8,000 Hz. These frequency ranges are chosen based on the response of TCS structures to harmonic excitation, which will be shown later in this chapter. For the purpose of a uniform beam vibration analysis, the frequency ranges that will be considered are the low and mid frequency ranges, since the response at the high frequency range will only be affected by the trusses in a TCS structure. The response of a structure to a time-harmonic excitation can be modelled in terms of modal expansion such that the response at each frequency is determined by a summation of all the modal terms as discussed in Chapter One. Theoretically, an infinite number of modal responses are required to determine the exact structural response; however, the higher frequency modal components have a small contribution to the frequency response of a structure, and therefore only a limited number of modal terms are required to approximate the correct response of a structure in practice. In this analysis, the first 15 modes will be used to estimate the frequency response of a uniform beam under a time-varying load. As a comparison, the typical ratio of time-dependent displacement of a point on a beam between the 15^{th} mode and the 1^{st} mode is in the order of 10^{-6}, therefore 15 modes is sufficient to provide the necessary accuracy in this part of the analysis. Note that due to the nature of the harmonic loading and the boundary condition, only the symmetric modes, or the odd modes, are required since the contribution of the anti-symmetric modes, or the even modes, are equal to zero. In addition, a discrete number of data points will be used to determine the RMS velocity of a

specific beam structure design. If too few data points are used, the response may not be representative. However, if too many data points are used, computational efficiency for the thousands of FEA simulation runs may suffer. In order to explore this issue further, a beam with the parameters listed in Table 1 is analysed:

E	G	ρ	l	w	h	κ	υ	I
[GPa]	[GPa]	$[kg/m^3]$	[m]	[m]	[m]	N/A	N/A	$[10^{-10}m^4]$
10	3.85	500	0.5	0.005	0.01	0.85	0.3	4.17

Table 1. Structural parameters for initial uniform beam forced vibration analysis

where E is the elastic modulus, G is the shear modulus, ρ is the density of the beam, l is the length of the beam, w is the width of the beam, h is the height, κ is the Timoshenko shear coefficient, and I is the moment of inertia of the beam. The first 15 natural frequencies, which are related to the resonant frequencies in this forced vibration analysis, are shown in Table 2. Plotting the RMS velocity versus the spatial location at specific excitation frequency, the results are shown in Figure 8 and 9. Due to the large difference in the response magnitudes between the forcing frequency near and far away from the resonance frequency, the responses are plotted in two separate graphs in order to show them more clearly. The near-resonance and off-resonance forcing frequency responses are shown in Figure 8 and Figure 9 respectively. It can be observed from Figure 8 that the center point along the length of the beam is a good indicator of the magnitude of RMS velocity level. However, at off-resonance excitation frequencies, if data is only taken at the center point, the results may not capture the overall RMS velocity level on the beam; this is evident from the RMS velocity distribution curve for the 640 Hz and 1380 Hz excitation frequency in Figure 9. For this reason, 15 data points with equal spatial intervals will be used to determine the average RMS velocity values. The comparison for the results between the single-point response, which is taken at the half-length point, and the 15-point average response is shown in Figure 10. It can be observed that the two anti-resonant frequencies predicted by the single-point response graph are in fact a local phenomenon and do not represent the overall structural response.

Due to the large range of RMS velocity magnitude in a single analysis, a log scale with the base of 10 is used for the response. The result clearly shows that high RMS velocity

magnitudes occur at the odd-mode natural frequencies, and it is at those frequencies that the structure is capable of radiating noise most efficiently. For this reason, it will be advantageous if the designer can control the natural frequencies of a TCS structure so that resonance does not occur for the vibration frequencies to which an aircraft is exposed during operation. The magnitude of the response is of secondary importance at this stage of the development because a unit load was used as a representative forcing term, and the beam analysis serves only as a means to determine general design guidelines for a TCS panel structure. For these reasons, the next analysis will be focused on determining the relationships between the natural frequencies of the beam, and the various structural parameters with simply supported boundary conditions and a time- harmonic pressure load.

Mode 1	**Mode 2**	**Mode 3**	**Mode 4**	**Mode 5**	**Mode 6**	**Mode 7**	**Mode 8**
81 Hz	324 Hz	726 Hz	1285 Hz	1995 Hz	2853 Hz	3852 Hz	4986 Hz
Mode 9	**Mode 10**	**Mode 11**	**Mode 12**	**Mode 13**	**Mode 14**	**Mode 15**	
6247 Hz	7629 Hz	9123 Hz	10723 Hz	12422 Hz	14211 Hz	16085 Hz	

Table 2. Natural frequencies of a uniform beam for the initial analysis

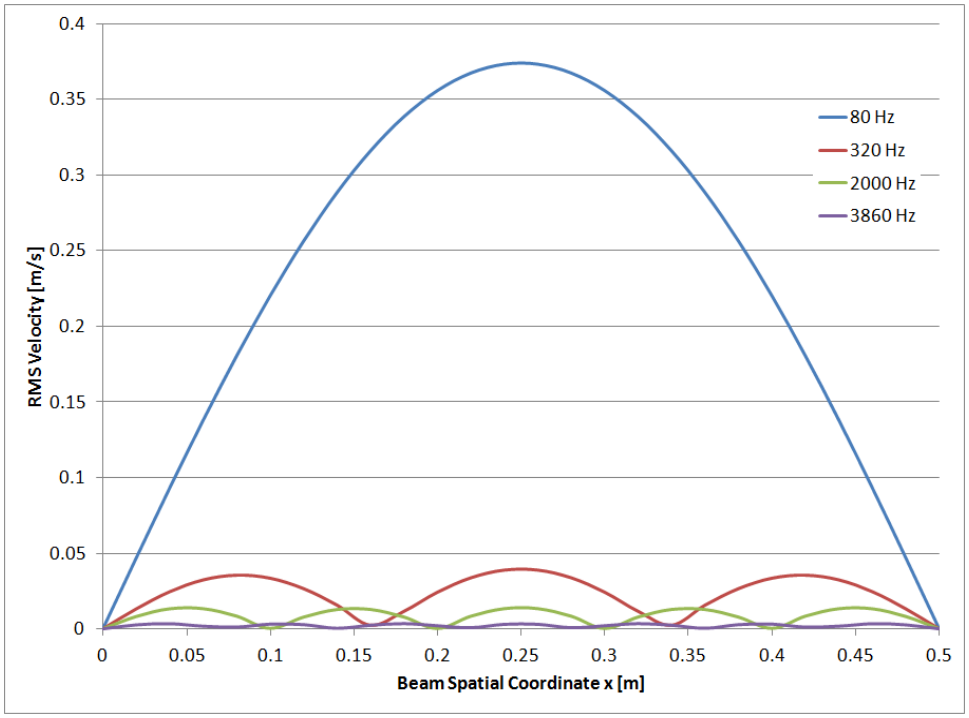

Figure 8. Time averaged RMS velocities for near-resonance excitation frequencies as a function of the spatial location for a uniform beam

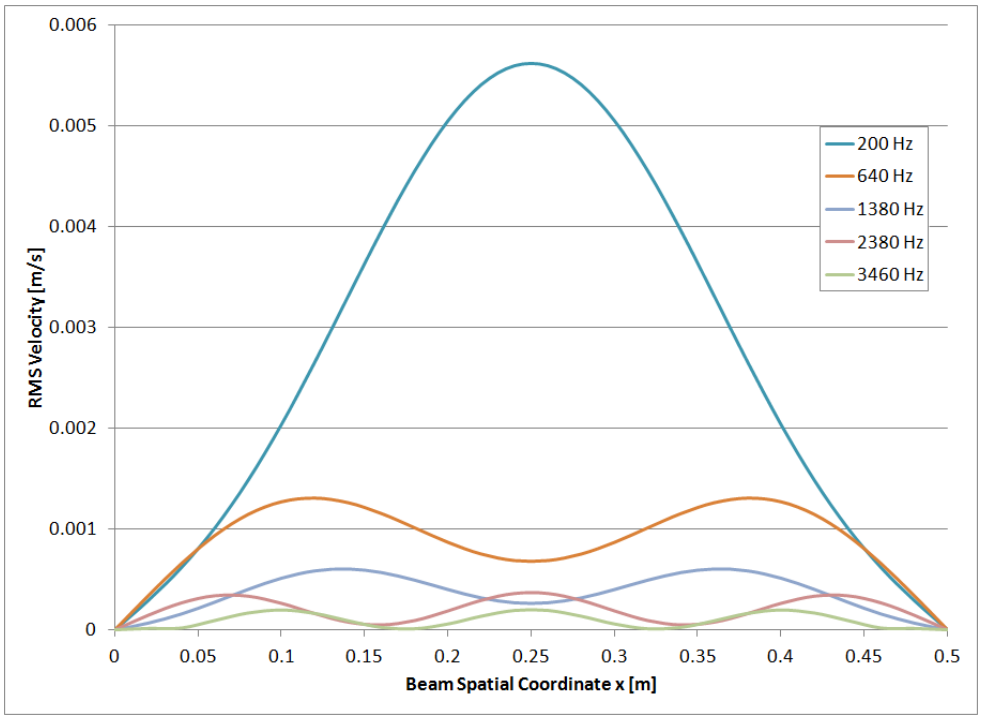

Figure 9. Time averaged RMS velocities for off-resonance excitation frequencies as a function of the spatial location for a uniform beam

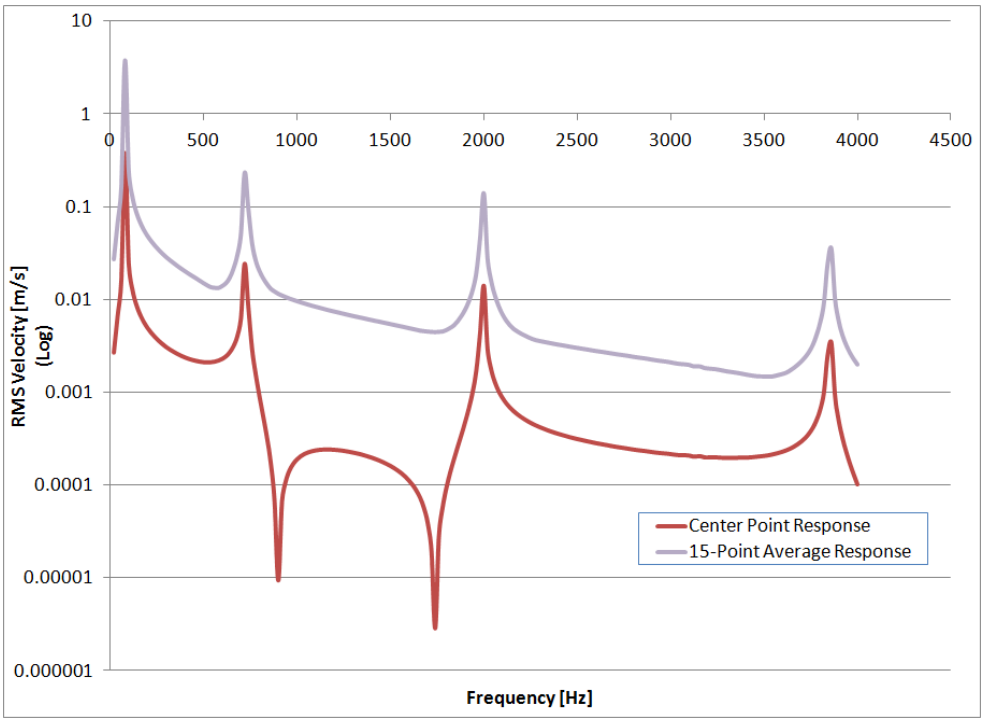

Figure 10. Comparison between beam's center response and 15-point average response

In order to increase the confidence level of the theoretical analysis, a finite element model is created in order to determine the correspondence between theory and finite element simulation. Since the response of the beam is one-dimensional in the transverse direction and the beam has uniform properties, using beam elements to model the structure is sufficient to describe the response of the beam. The parameters for the FEA have the same values as shown in Table 1, and the result is shown in Figure 11. It can be observed that the FEA result and the theoretical result match closely, and the errors are primarily caused by random numerical noise associated with high frequency loads.

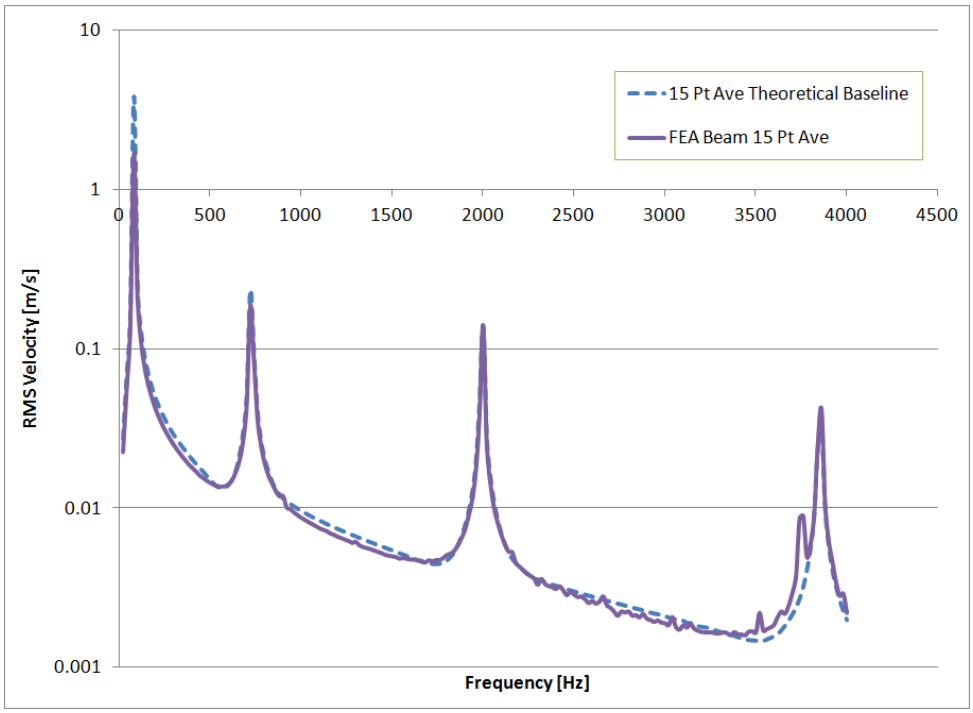

Figure 11. Comparison between theoretical beam's response and finite element analysis results using beam elements

3.1.2 Sensitivity and Parametric Studies of Uniform Beam Structure Using Theoretical Formulations

Using the structural parameters shown in Table 1 as the basis for parametric studies, the elastic modulus, shear modulus, density of the beam, and length of the beam are varied by $\pm 75\%$ from their base values. The changes in the natural frequencies for the first ten modes are shown in Figure 12 to Figure 15 in order to illustrate the sensitivity of the response upon a change in the parameter. It should be noted that the minimum or maximum values of the natural frequencies are normalized to provide a basis of comparison. It can be observed in Figure 12 that by

increasing the Young's modulus of a simply supported uniform beam, the natural frequencies of all the modes increase significantly at approximately the same rate, with the higher modes increasing at a slightly slower rate at high Young's modulus values. On the other hand, as the

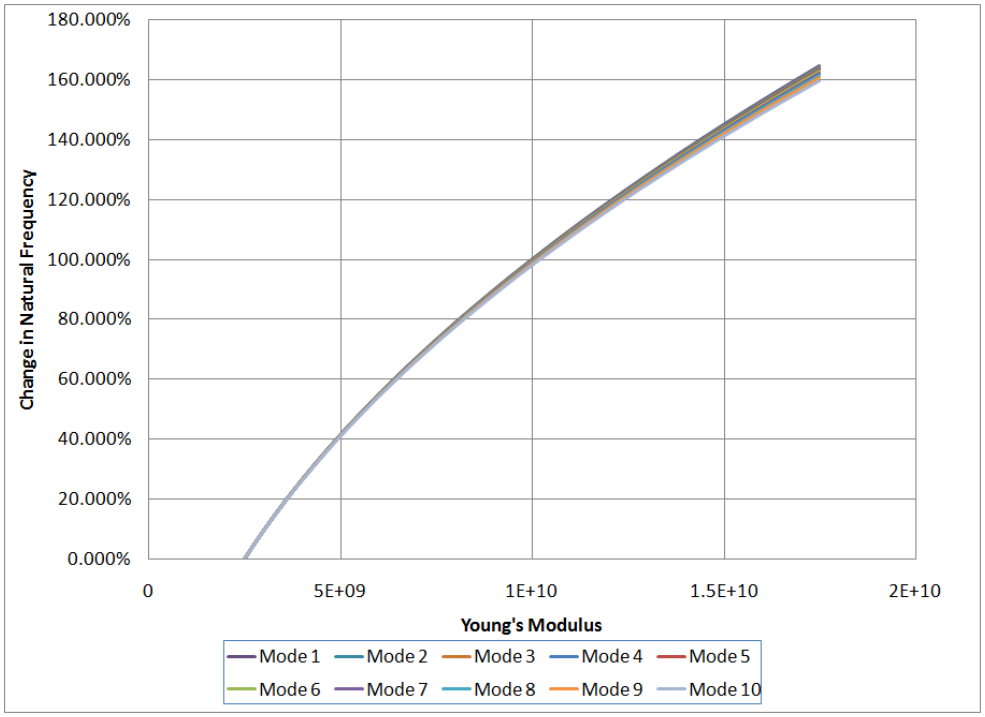

Figure 12. Parametric study for varying the Young's modulus by $\pm 75\%$ for the first 10 modes

Young's modulus decreases, the natural frequencies of all the modes decrease at the same rate. Changes in the elastic modulus represent changes in the elastic stiffness of a beam structure, which can be achieved by changing the face-sheet thickness and material properties, as well as individual truss dimensions and material properties. The sensitivity of the latter will depend on the particular design of the truss configurations and the orientations.

Figure 13 shows the effect of varying the shear modulus. The natural frequencies vary linearly with the modes of vibration and non-linearly with the shear modulus. As the shear modulus increases, there is an increase in the natural frequencies. However, the rate of change of the natural frequencies diminishes, and this effect is more prominent at higher modes. The fact that the rate of change of the natural frequencies is different for different modes is advantageous because a designer can target a specific natural frequency and modify the shear modulus of a TCS structure to change the natural frequency to a desired value. Figure 14 shows

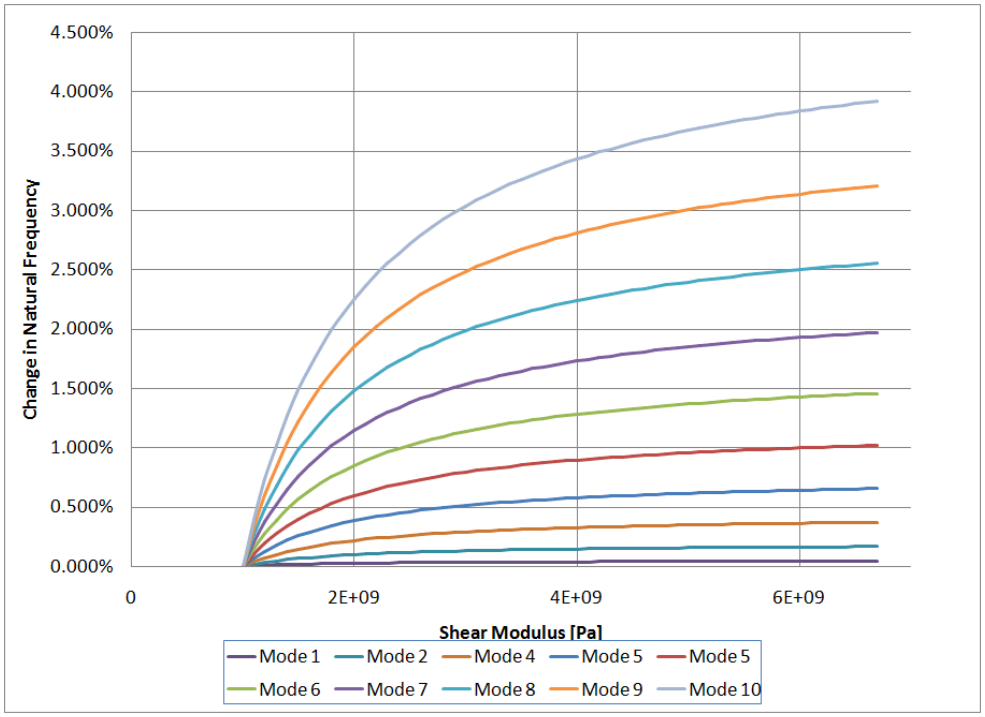

Figure 13. Parametric study for varying the shear modulus by $\pm 75\%$ for the first 10 modes

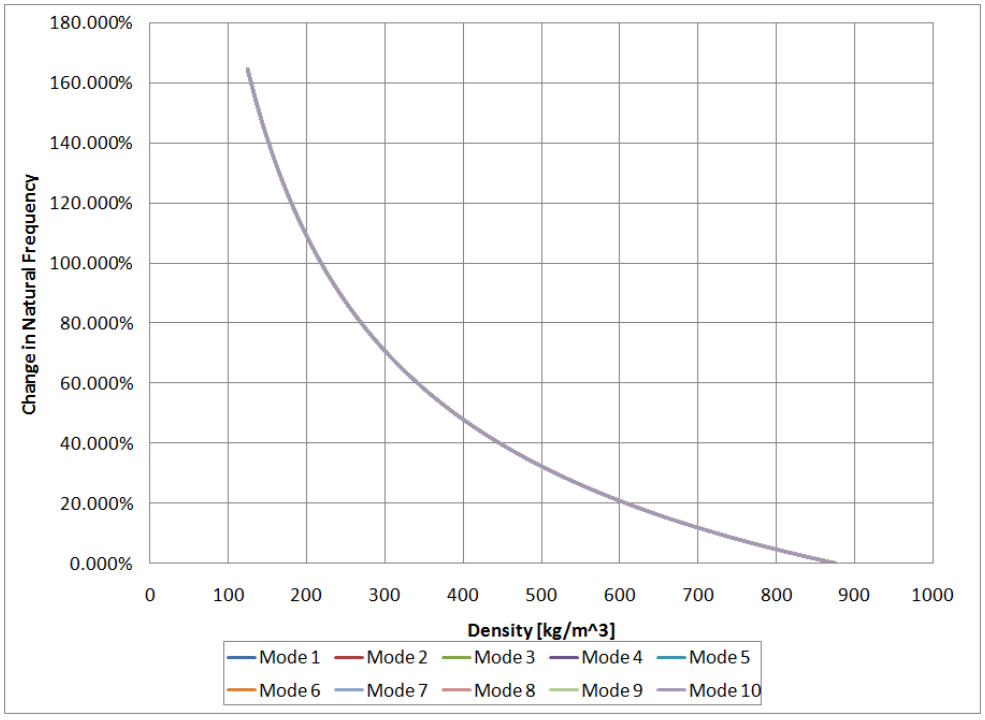

Figure 14. Parametric study for varying the density of the uniform beam by $\pm 75\%$ for the first 10 modes

the result of changing the density of a uniform beam structure. The natural frequency of all modes increased exponentially as the density decreases. This result illustrates another advantage of TCS structures because TCS panels can achieve higher structural strength than structures with uniform properties for the same amount of mass. Therefore the natural frequencies can inherently be shifted higher, which is a common objective of acoustic panel design. Last, the parametric study for the length of a beam, as shown in Figure 15, demonstrates that a decrease in the length of the beam will cause an increase in the natural frequencies of the system, and an

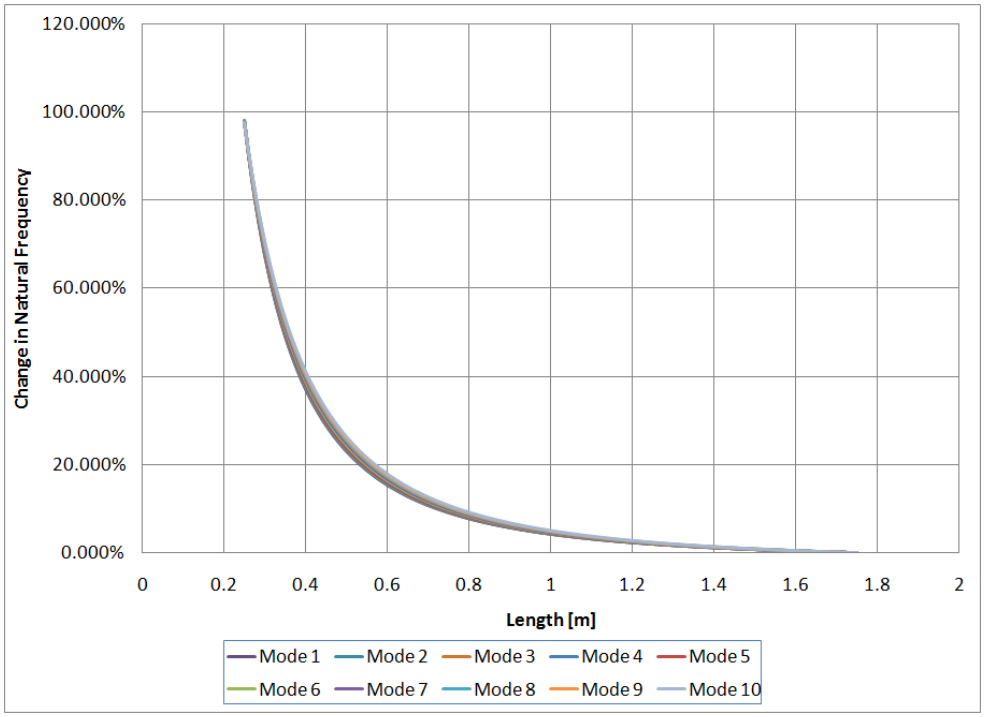

Figure 15. Parametric study for varying the length of the uniform beam by $\pm 75\%$ for the first 10 modes

increase in the length of the beam will cause a decrease in the natural frequencies. Changing the length of a beam is equivalent to changing the boundary support of the panel on an aircraft. Therefore this information gives the designer another tool to tailor the acoustic characteristics of a TCS panel.

3.2 Finite Element Analysis of a TCS Structure

3.2.1 Finite Element Model for a TCS Structure

Although the results from the previous sections demonstrated a number of means to control the vibro-acoustic characteristics of a beam structure, how these means can be applied to the design of a TCS structure, and how the core unit cell design can change the overall structural acoustic behaviour have not been addressed. One of the reasons for that is that the analysis tool that is available is analytical, which neglects the inhomogeneity of a TCS structure. The complex geometry of a TCS structure makes it difficult to develop a fully analytical solution; therefore a numerical approach needs to be employed. Due to the nature of the problem, a finite element approach will be used to analyze the TCS structural response. Various considerations regarding the FEA were presented in the previous chapter. There are four base structures that are being analyzed in this research; the difference between them are in the design of their unit cells, while the material and dimensions for the pair of face-sheets are identical for all the base structures. The four different unit cell designs are: the diagonal array, the tetrahedral, the pyramidal, and the Kagome unit cell designs. The finite element models of these designs are shown in Figure 16. Each of these TCS beam structure is composed of repeating unit cells with a dimension of 1 cm width by 1 cm length by 1.5 cm height. The trusses are made of pultruded carbon rod with a diameter of 1 mm. Each face-sheet is 2 mm thick and is assumed to be made up of 3 plies of cross-woven carbon fibre fabric bonded together by an epoxy matrix. Since the carbon fibre sheet is plain woven, and all the plies have the same orientations, orthotropic material properties are used. It is assumed that the deflection of the beam is small during the loading process and hence a homogeneous linear elastic model can be used to describe the material behaviours in the FEA. The specific properties for the carbon rods and the face-sheets are listed in Table 3. ABAQUS Explicit was used as the solver for these FEA models due to the nature of the required simulation. The study period is set to 0.2 s in order to incorporate the lowest frequency case and to provide sufficient data for the RMS velocity values. The time-step is set automatically by ABAQUS, which is determined by the smallest element in the model and the time-scaling factor. Linear quadrilateral thin shell elements are used to model the face-sheet, and linear beam elements are used to model the truss core. Reduced integration elements are used in order to reduce simulation run-time, and to prevent non-physical overly stiff response, such as shear locking. Five integration points through the thickness of the shell are used in order to capture the

correct bending behaviour and the elastic rebound of the structure during its deformation. The number of triangular elements is kept to a minimum in order to prevent non-physical stiff behaviour. The two-noded beam element has an integration point at the center of the beam, and the trusses are assumed to be rigidly bonded to the face-sheet at their ends. Damping is assumed to be negligible, and for the purpose of this research, ignoring damping will not affect the outcome. Simply supported boundary conditions are applied to the model by restraining the *x*, *y*, and *z* translational freedom at the edge of the bottom face-sheet. The simulations are all run in a quad-core desktop computer with a Gentoo Linux operating system in order to prevent cross-platform inconsistency. In order to perform a frequency response analysis for each TCS design, the time-harmonic unit pressure load is applied to the surface of the top face- sheet at the range of frequency between 20 Hz to 4000 Hz with a 20 Hz increment.

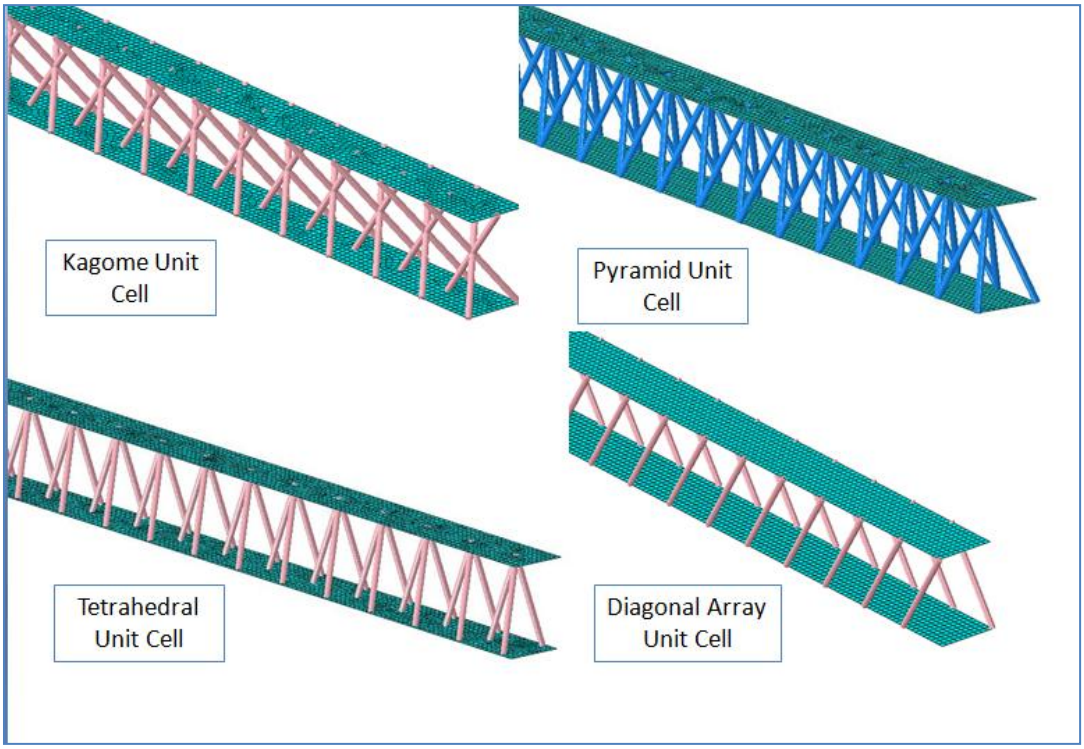

Figure 16. Various TCS beam structure designs – Kagome, pyramid, tetrahedral, and diagonal array unit cell designs

These loading profiles are generated by a C++ code, which lets the user specify the frequency of the load, the magnitude of the load, and the number of data points to represent the loading profiles. Another C++ program is developed to generate the Python scripts to initiate the

	Density $[kg/m^3]$	Elastic Modulus [GPa]	Poisson Ratio
Pultruded Carbon Rod	350	140	0.1
Face-Sheet	1120	60	0.1

Table 3. Mechanical properties for pultruded carbon rod and carbon composite face-sheet

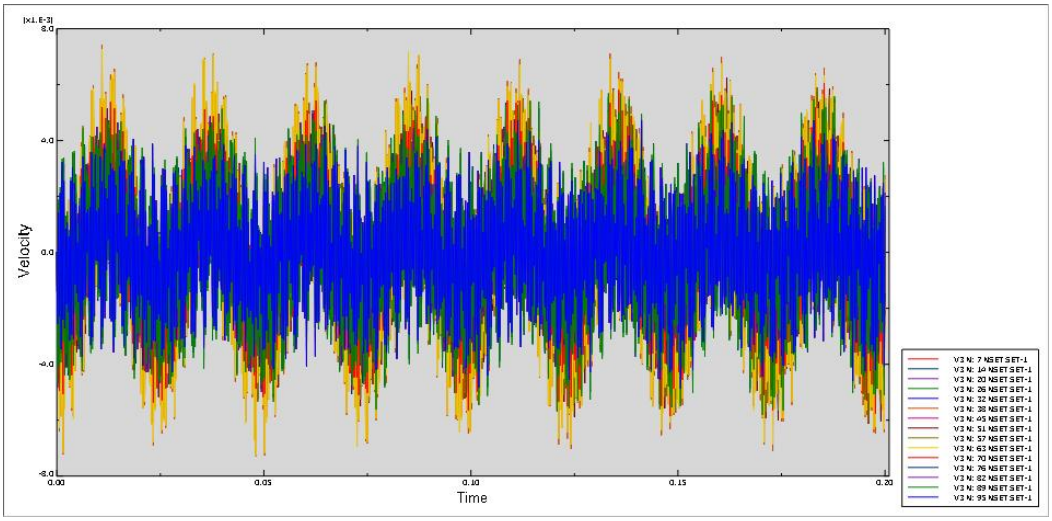

Figure 17. Typical multi-point response from forced vibration analysis in ABAQUS (each color represents a response at a different location)

simulation runs in ABAQUS. The transverse or out-of-plane velocity responses on the bottom surface are recorded for the 15 nodal points, which are evenly spaced along the length of the beam. A typical simulation result from ABAQUS is shown in Figure 17. The results are then imported into a C++ program for post-processing. The RMS velocity values are obtained from this program and the results are plotted in a graph similar to the one presented in Figure 11.

3.2.2 Static Finite Element Analysis

Before any dynamic FEA is carried out for frequency response analysis, a static FEA can be performed to determine the deflection of the beams under a quasi-static pressure. Knowing the deflection, the effective structural properties of a beam can be determined, such as the apparent elastic modulus, apparent density, and the apparent bending stiffness. A unit, ramp-up quasi-static distributed pressure load was used in these static finite element analyses. The same finite

element meshes and boundary conditions are used in the model. The resultant deflection is recorded, and using the classical bending theory, the deflection can also be represented by:

$$w_{max} = -\frac{5ql^4}{384EI}, \tag{3.1}$$

where w_{max} is the maximum deflection at the center of the beam, q is the load per unit length of the beam, l is the length of the beam, E is the elastic modulus, and I is the moment of inertia. Using this equation, the approximated, effective bending stiffness of the beam, EI, can be determined. Assuming that only the face-sheets contribute to the moment of inertia, the moment of inertia, I, can also be determined, and therefore the effective elastic modulus can be calculated. The results of these analyses for all the models considered in this research are shown in Table 5, and the corresponding TCS design attributes are listed in Table 4. Using the effective elastic modulus obtained from these analyses, the effective shear modulus can be calculated using elasticity theory, assuming a Poisson's ratio of 0.3. Assuming an effective cross-sectional area equals to a uniform beam (0.01 m x 0.015 m), and an effective density calculated using the overall mass and a representative uniform beam volume, the first mode natural frequency for each design configuration is calculated and presented in Table 5. It was found that these natural frequency values are in close agreement to the first mode resonant frequencies determined from the frequency response analyses, which will be presented in the next section.

3.2.3 Dynamic Finite Element Analysis and Frequency Response Analysis

The results of the frequency response analyses for the four base TCS beam designs are shown in Figure 18. Figure 18 shows the response in terms of RMS velocities, and Figure 19 shows the response in terms of decibel, which is obtained by [29]:

$$Response\ [dB] = 20log_{10}\left[\frac{\omega}{\dot{w}_{ref}}\sqrt{\left(\frac{1}{m}\sum_{k=1}^{m}\dot{w}_k^2\right)}\right], \tag{3.2}$$

where $\dot{w}_{ref}$ is a normalizing reference velocity, which is equal to 5×10^{-8} m/s [29]. The response will be measured in RMS velocity for the on-going analysis in order to be consistent and to emphasize the relative nature of the results. It can be observed that most of the four

designs have a similar first resonance, which is around 400 Hz. This similarity is due to the similarity in their effective elastic modulus, despite the difference in unit cell design. This is also evident from their free vibration response. It is observed that the first mode is strongly dependent upon the effective bending stiffness, which has a weak dependency on the core design. This phenomenon can be clearly seen by comparing the baseline pyramid, Kagome, and the tetrahedral unit cell designs. Figure 20 shows the mode shapes of a typical TCS beam structure. It can be observed that the unit cell barely deforms in the low natural frequencies and the deformations in the unit cell increase at higher modes. At the Low Frequency (LF) range, the dynamic response may be estimated by homogenization techniques as illustrated previously.

TCS Design	TCS Name	Face-Sheet Thickness [mm]	Pin Diameter [mm]	Attributes
1	Pyramid	2	1	Baseline unit Cell design
2	Kagome	2	1	Baseline unit Cell design
3	Tetrahedral	2	1	Baseline unit Cell design
4	Array	2	1	Baseline unit Cell design
5	Array 1.5	2	1	[4] design with 11° pin angle increase over [4]
6	Tetrahedral Packed Edge	2	1	[3] design with 1.1 spatial distribution factor for unit cell
7	Tetrahedral Packed Center	2	1	[3] design with 0.9 spatial distribution factor for unit cell
8	Tetrahedral Heavy Pins	2	1	[3] design with increased pin density to match [1]
9	Tetrahedral Heavy Face-sheet	2	1	[3] design with double the face-sheet density
10	Tetrahedral Thick Face-sheet	4	1	[3] design with 4 mm thick face-sheets
11	Tetrahedral Thin Face-sheet	1	1	[3] design with 1 mm thick face-sheets
12	Tetrahedral Thick Pins	2	1.5	[3] design with 1.5 mm diameter pins

Table 4. TCS designs and their attributes

In the Mid- Frequency (MF) range, intracell resonance begins to take place, causing the cell members to deform, therefore there is a mixed deformation mode between the overall beam and the unit cell in this frequency range. At High Frequency, most of the deformation occurs at the cell level. Although most of the designs have a similar first resonant frequency, the array unit cell first resonance occurs at only 160 Hz. The main reason for such a low first resonant frequency for the array design is because of its low bending stiffness, as shown in Table 5. For

TCS Design	Deflection [nm]	Overall Mass [g]	Overall Density $[kg/m^3]$	Bending Stiffness EI $[N \cdot m^2]$	Shear Modulus $[MPa]$	Elastic Modulus $[GPa]$	1st Natural Frequency [Hz]
1	0.419	23.3117	310.823	194.385	241.588	85.897	405.704
2	0.409	23.2145	309.527	199.185	384.098	88.018	411.541
3	0.520	23.0518	307.357	156.628	45.425	69.213	366.225
4	2.910	22.8956	305.275	27.919	99.697	12.337	155.145
5	2.493	22.9831	306.441	32.633	487.630	14.420	167.413
6	0.536	23.0518	307.357	151.945	86.182	67.143	360.708
7	0.709	23.0518	307.357	114.770	75.874	50.716	313.492
8	0.552	23.3117	310.823	147.439	45.425	65.152	353.333
9	0.52	45.4518	606.024	156.628	45.425	69.213	260.810
10	0.308	45.4518	606.024	263.860	61.761	57.278	338.514
11	1.03	11.8518	158.024	78.745	27.537	69.892	362.146
12	0.444	23.8667	318.223	183.179	69.199	80.945	389.230

Table 5. Effective mechanical properties of various TCS designs from static FEA

this reason, it is important for a structure to have sufficient bending stiffness if one is to avoid having a low first resonant value. Despite the similar first resonant frequency for the pyramid, Kagome, and tetrahedral unit cell designs, their second resonance frequencies are significantly

different from each other, ranging from 1680 Hz for the tetrahedral unit cell design to 2340 Hz for the Kagome design. The pyramid unit cell has a second resonant frequency at 2240 Hz. This represents a 33% difference between the tetrahedral and the pyramid designs. Such significant change in performance was achieved without modifying the material, the unit cell dimension, the beam dimension, the diameter of the pins, or the thickness of the face-sheets. This demonstrates the design flexibility provided by the TCS structure configurations. Due to this large performance gradient, their proximity to the coincidence frequency, and the relative ease of fabrication, it was decided that these two designs will be fabricated into two TCS panels for experimentation in an acoustic chamber. The details of these experiments will be presented in Chapter Four. Regarding the array design, it also has a high modal density even at the low frequency excitation range, therefore it is not a good TCS structure design along with the other short-comings mentioned previously. However, the pin angle in the array design can be easily changed independently without affecting the other structural parameters, therefore it has some advantages in terms of being a subject of parametric studies.

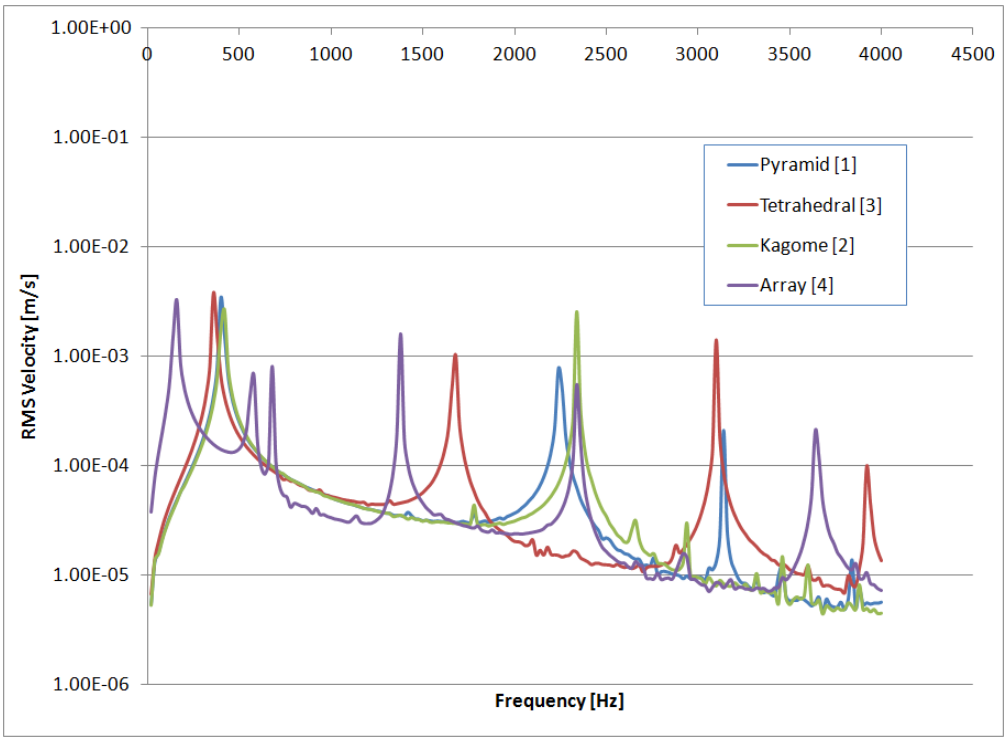

Figure 18. Frequency response analysis for four base TCS beam designs measured in RMS velocity

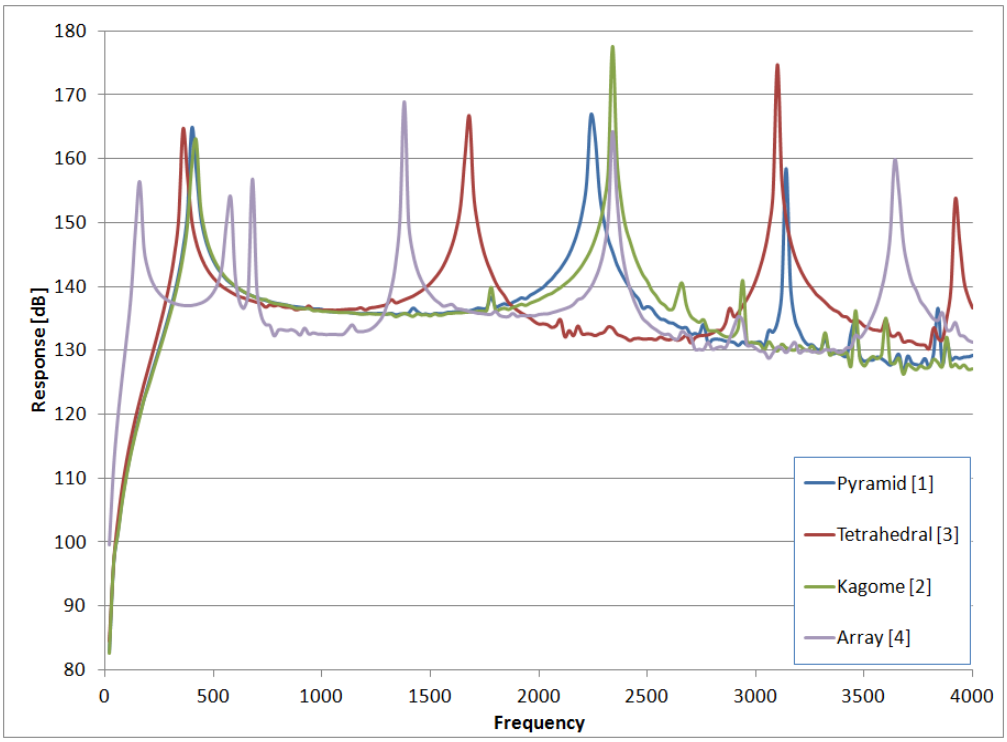

Figure 19. Frequency response analysis for four base TCS beam designs measured in decibel

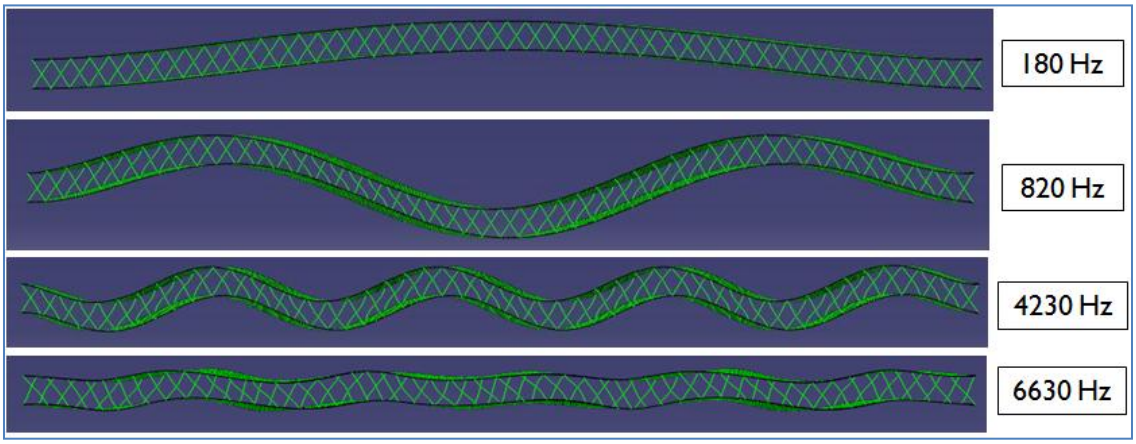

Figure 20. Mode shape and deformation pattern for a typical TCS beam structure

In the next analysis, the pin angle of the array unit cell design will be changed from 56° to 45°. This change in the pin angle has an effect on the shear properties of the TCS beam structure. The lower the pin angle, the higher the shear stiffness is expected. The result of this analysis is shown in Figure 21. Considering the results from the static FEA analysis, a 19.6% decrease in pin angle corresponds to 16.8% increase in the effective elastic modulus and a 389% increase in the longitudinal effective shear modulus. This result indicates that an increase in the

shear stiffness can be achieved by reducing the pin angles, which is a result of changing the component of the load vector along the pins. In addition, the resonant frequencies starting from the second resonant peak shifted to higher values, which is desirable in some applications.

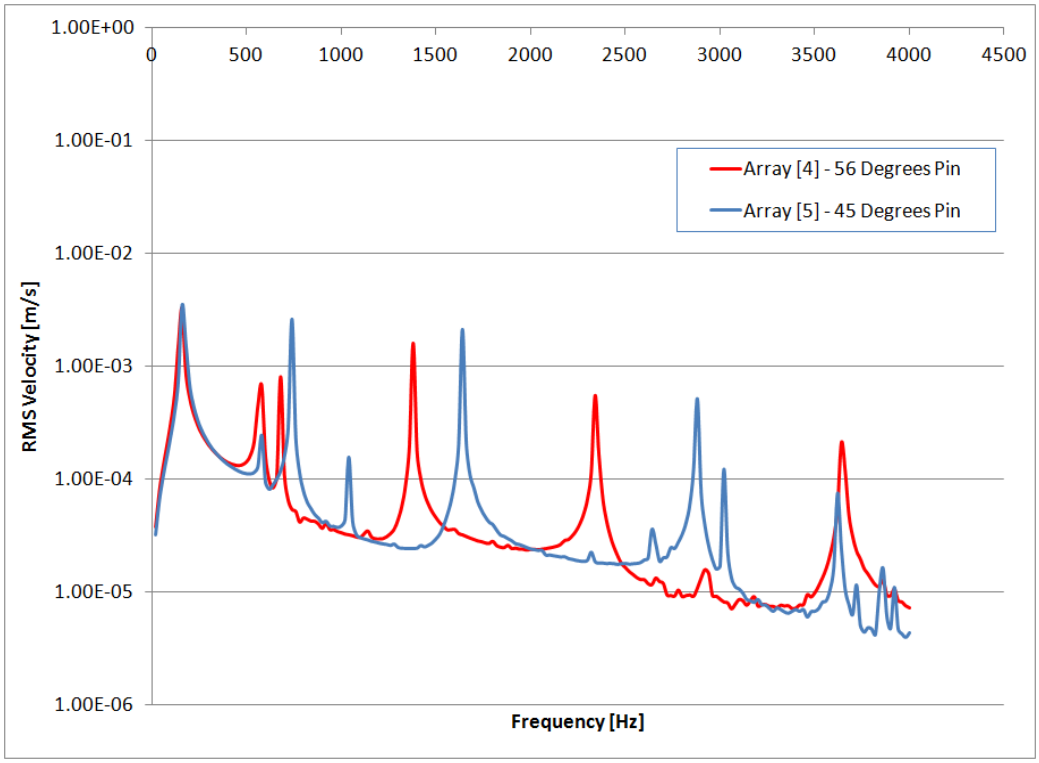

Figure 21. Frequency response analysis for diagonal array unit cell design with different pin angles

However, there are other practical concerns regarding the design of the pin angles, such as compression stability, compressive strength, and spatial limitations. Due to the low structural stiffness, and the low first resonant frequency of the array unit cell design, it is not a practical design for a TCS structure. One of the reasons that the array design performs poorly is the lack of multi-dimensional stiffness. The pins are only oriented in the *XZ*-plane, and therefore it does not provide sufficient bending stiffness for a beam or a panel structure during a vibration load. The other three unit cell designs, pyramid, Kagome, and tetrahedral unit cells designs, do not have this short-coming. Due to the structure of the unit cell design, and the nature of these analyses, the various structural parameters of a tetrahedral unit cell design can be varied independently and easily to explore their effects on the overall TCS structure's vibro-acoustic performance.

In the next analysis, the truss core properties of the tetrahedral unit cell design will be changed by modifying the pin diameter. Two different pin diameters will be studied in these analyses; 1 mm, which is the original diameter, and 1.5 mm. The frequency response analysis is shown in Figure 22. The quasi-static analyses show that the bending stiffness of the 1.5 mm pin tetrahedral is increased by 17% while the weight is only increased by 3.5%. As a result of this structural performance improvement for a minimal weight increase, the first resonance mode frequency only increased slightly, however the magnitude of the first peak also decreased. As mentioned before, these peaks are responsible for high acoustic radiation, therefore the primary design objective of TCS structure should be to avoid any coincidence. Even if the response magnitude at these resonance peaks is lowered, the overall performance of the TCS panel will suffer. For these reasons, the secondary objective of a good TCS design is not in lower peak response magnitude, but in low modal density. The higher the modal density, the more

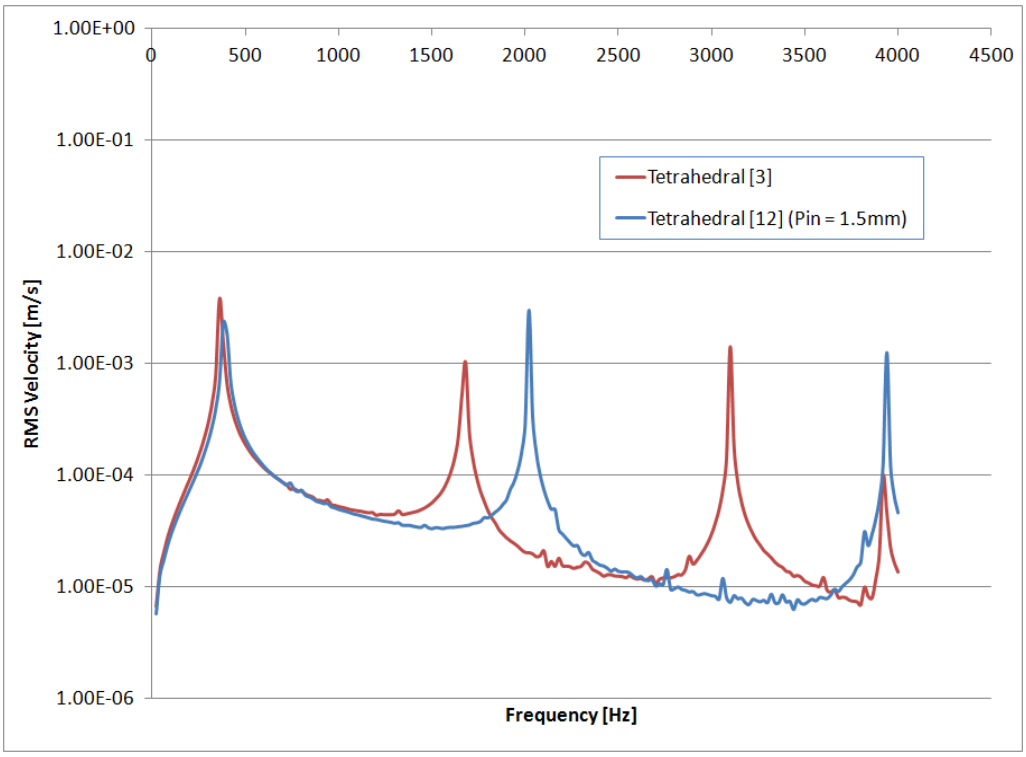

Figure 22. Frequency response analysis for tetrahedral unit cell design TCS beam with two different pin diameters

resonance occurs in a given frequency range, and therefore there are more opportunities that the external pressure frequency will coincide with the natural structural frequency, causing resonance. The tetrahedral design with 1.5 mm diameter pins decreased its modal density by approximately 19.5% in the low frequency range, which indicates a significant improvement over the baseline Tetrahedral design.

The increase in pin diameter corresponds to an increase in the load carrying capacity of the structure, as well as the mass of the core. In order to distinguish which parameters affected the previously observed performance differences, only the density of the pin will be increased in the next analysis. For this reason, the effect of the mass of the core or the pins will be investigated next. In addition, the pyramid unit cell design shows a higher elastic modulus value and first resonance frequency than the tetrahedral design; however it also has a higher core mass. For these reasons, the pin density of the core of a tetrahedral baseline design will be increased to match the core weight of the pyramid design. The comparison of the "heavy" pin design, the baseline tetrahedral unit cell design, and the pyramid unit cell design is shown in Figure 23. It

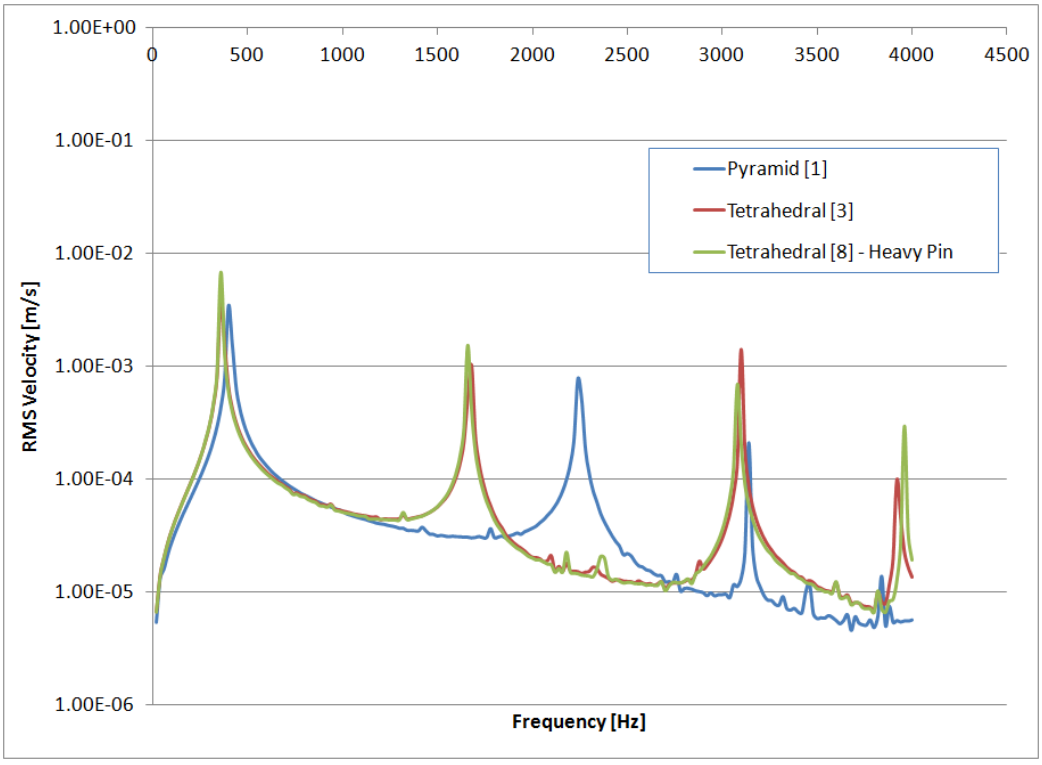

Figure 23. Frequency response analysis for tetrahedral unit cell design TCS beam with heavy pin design

can be seen that performance of the "heavy" pin design does not alter much from the original tetrahedral unit cell design, and therefore it can be concluded that the improved performance of the 1.5 mm diameter pin and the pyramid unit cell design is not due to the increase in mass.

Another parameter that can be changed in order to modify the structural-acoustic performance of a TCS structure is the spatial distribution of the unit cells. In this analysis, two different cases are considered and they will be compared to the tetrahedral baseline result. The first case is a design with an expansion factor of 1.1 from the edge of the tetrahedral design, and the second case is with a contraction factor of 0.9. These designs are shown in Figure 24, and their performances are shown in Figure 25. The quasi-static analyses showed that, while the expanding unit cell design has a similar bending stiffness as the baseline case, the contracting unit cell case has a 26.7% drop in the elastic modulus value. Although the first resonance frequencies for the three designs are similar, the spatially varying unit cell designs have gradually lower resonant frequencies as well as higher modal densities. It is observed that both the expanding and contracting spatially distributed unit cell designs have a lower effective stiffness than the evenly spaced unit cell design, and it is shown that the two spatially distributed unit cell designs have higher modal densities.

Although the previous analyses have been focused on the design of the core, the effect of the face-sheets on the dynamic response of the structure cannot be ignored. In the following analysis, the thicknesses of the face-sheets will be varied. In the first case, the face-sheets for a baseline tetrahedral unit cell beam will be reduced from 2 mm to 1 mm, and in the second case, the thicknesses will be increased to 4 mm. The results are shown in Figure 26. It can be

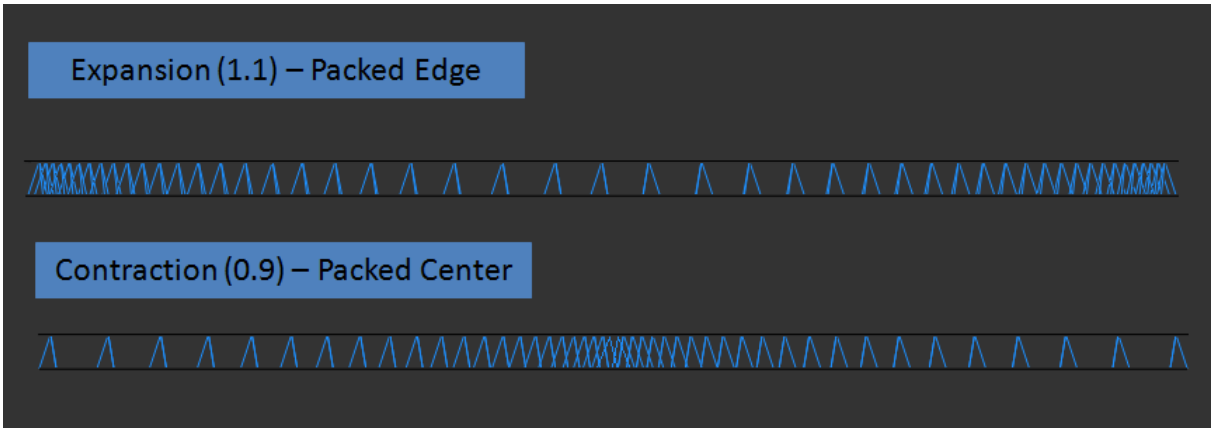

Figure 24. Tetrahedral unit cell designs with spatially varying unit cell distances

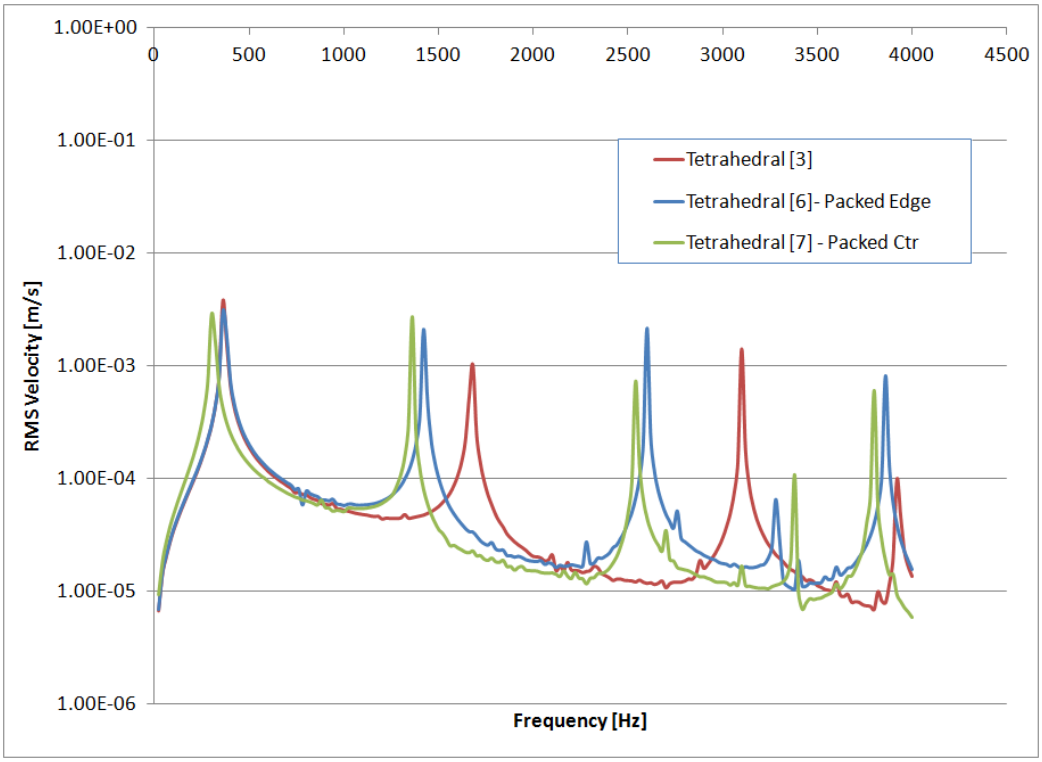

Figure 25. Frequency response analysis for tetrahedral unit cell design TCS beam with spatial unit cell distribution

observed that the magnitude of the responses show a clear distinction between the three cases. The thinner face-sheet design shows a higher RMS velocity than the baseline case, and the thicker face-sheet design shows a lower RMS velocity value. This corresponds to the mass law of vibrating structures, which states that the transmission loss or the RMS velocity is determined primarily by the excitation frequency and the mass per unit area at an excitation frequency away from the natural frequency. The thicker face-sheet design represent a 95.8% increase in mass and a 68.5% increase in bending stiffness, and the thinner face-sheet design shows a 48.6% decrease in mass and a 49.7% decrease in bending stiffness. The response of the "heavy" face-sheet design is also plotted in Figure 26 for comparison. The "heavy" face-sheet design has the same weight as the thick face-sheet design, which was obtained by doubling the face-sheet density of the tetrahedral unit cell design. These results indicate that varying the thickness of the face-sheets has a significant impact on the weight and static stiffness value of the system. However, the changes in the modal density and the resonance frequency are not as large as those caused by changing the core parameters, such as the pin diameter and the unit cell designs.

By increasing the density of the face-sheets without increasing their stiffness, the first resonant frequency is lowered, this is shown in Figure 27. In addition, all the other subsequent resonant frequencies are lowered and the modal density is decreased. This may be an undesirable situation, therefore it may be important to increase the stiffness of the face-sheet without significantly increasing the mass of the face-sheets to increase the first resonant frequency if reduction of the modal density of the frequency spectrum is to be realized.

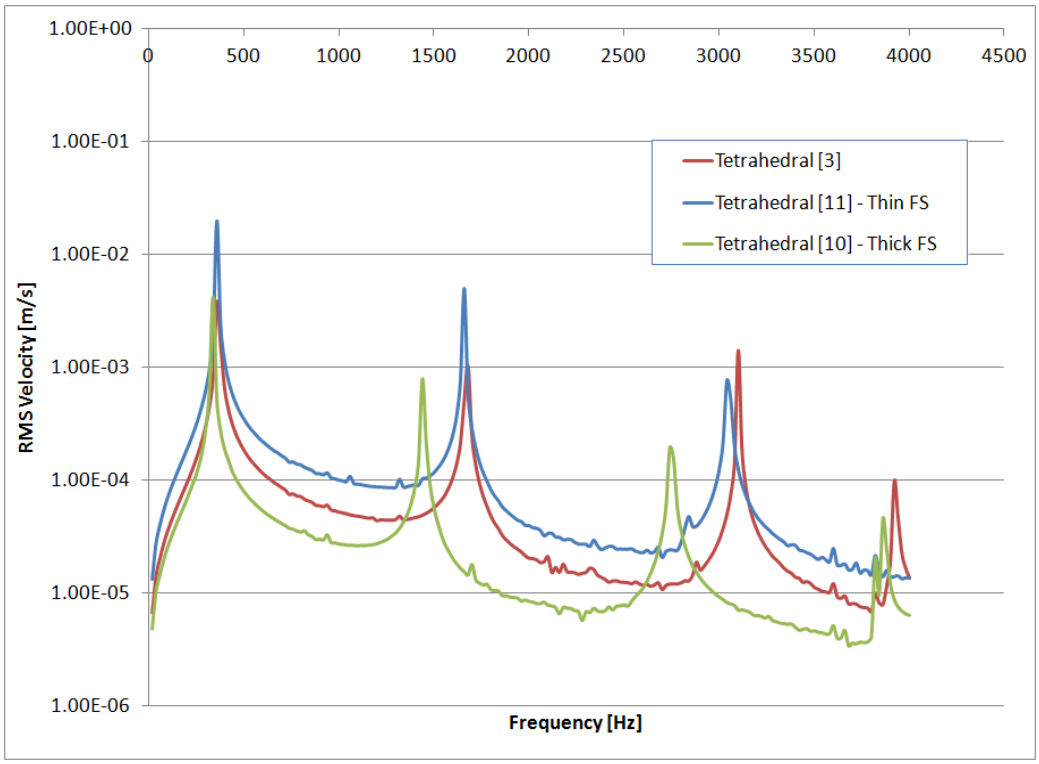

Figure 26. Frequency response analysis for tetrahedral unit cell design TCS beam with various face-sheet thicknesses

The frequency response analyses that have been done for this research explored the various interactions between the structural parameters and the vibro-acoustic performance of a number of TCS structure designs. Table 6 summarizes the general findings of these analyses. These findings only serve as a general guideline when designing a TCS panel structure. The specific performance of the design needs to be analyzed by FEA, and possibly a fluid-structural interaction (FSI) FEA, where the acoustic field is coupled with the structural response. However, certain observations were made. In the unit cell level, the modal density seems to decrease with the number of trusses. Each of the diagonal array, tetrahedral, pyramid, and

Kagome TCS structure design has two, three, four, and six rods in their unit cell design respectively, and their modal density decreased accordingly. This may suggest higher rigidity in the unit cell level will reduce the modal density, giving designer a favourable performance for acoustic noise reduction. This phenomenon can also be seen in the results of the static FEA – high modal density corresponds to designs that have high effective bending and shear stiffness. This results shows that a static stiffness analysis will be able to reveal a number of characteristics of a TCS structure design in terms of its vibro-acoustic behaviour. One of the variables in a TCS structure that is not captured in the summary shown in Table 6 is the specific unit cell design. This is due to the difficulties in representing the design in a parametric manner. Note that the TCS unit cell designs investigated in this research only represents a small number of the possible configurations. These designs were selected for the analyses due to their distinct difference in structure and performance. It can be seen that the change in unit cell designs altered the first resonant frequency the most, while changes in the unit cell level parameters change only the modal density and the higher resonant frequencies. In order to properly assess the performance of other TCS unit cell designs, similar analyses, as shown in this report, can be carried out, and

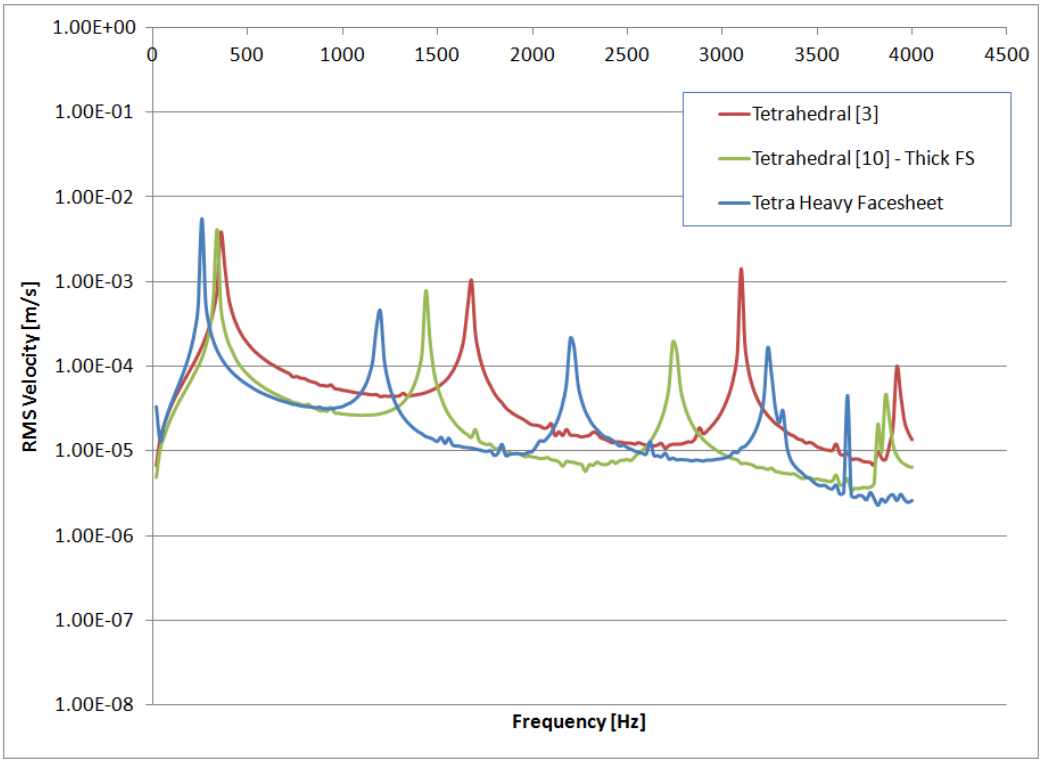

Figure 27. Frequency response analysis for tetrahedral unit cell design TCS beam with various face-sheet thicknesses and densities

	Quantities to be Increased				
	Pin Angle	Pin Diameter	Pin Mass	Spatial Distributed	Face-sheet thickness
First Resonance	Same	Slightly Higher	Similar	Similar	Similar
Second Resonance	Lower	Higher	Similar	Lower	Lower
Magnitude of Noise	Similar	Similar	Similar	Similar	Lower
Modal Density	Higher	Lower	Similar	Higher	Higher

Table 6. Summary of TCS structure sensitivity analyses

the results from this research can be used to determine the general trend in their vibro-acoustic performance for the application of reduction of cabin noise. It should be emphasized that only the TCS beam structures were analyzed numerically in this research, but not TCS panel structures. It was assumed that a TCS beam structure can reveal important characteristics of its equivalent panel structure at a much lower computational cost. This assumption will be assessed in the next chapter – Experimentation.

Chapter 4

Experimentation

Acoustic experiments with TCS panels were conducted in order to compare the TCS beam analyses with the performance of a corresponding TCS panel. These experiments were performed in an acoustic chamber to determine the transmission loss of the panels. White noise is produced inside the acoustic chamber with a TCS panel inserted in its opening, and a sound intensity probe is used to determine the noise level spectrum on the outside surface of TCS panel. A sketch of the experimental setup is shown in Figure 28. The industrial partner for this research is Bombardier Aerospace and they provided access to their acoustic chamber at the Downsview site to carry out these experiments.

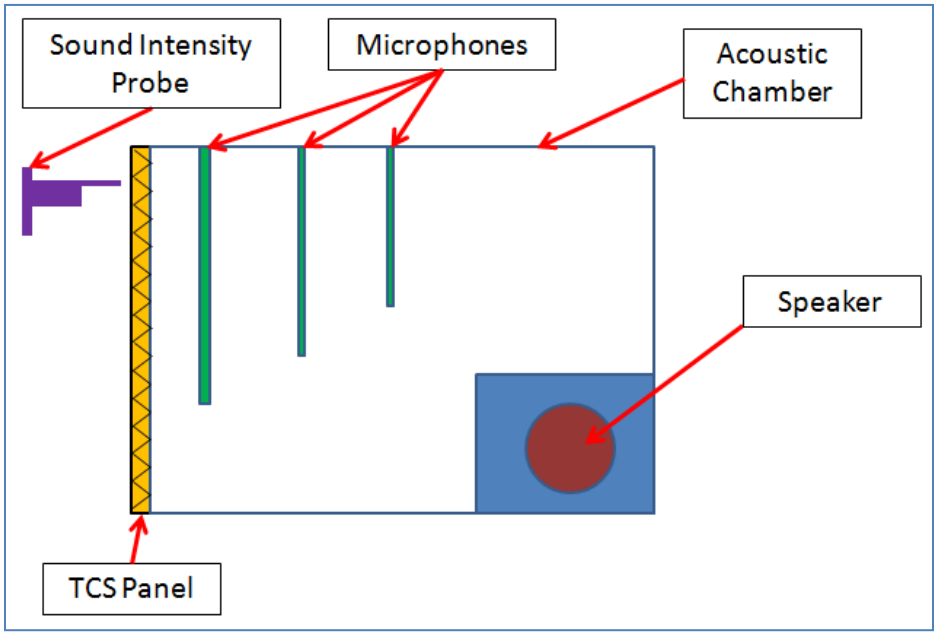

Figure 28. Side view of acoustic chamber experiment setup for TCS panel testing

4.1 TCS Panel Fabrication

Due to the complicated structure of a TCS panel, a robotic fabrication technique was used to create commercial TCS structures. However, because of the need to fabricate highly customised panels, an in-house method of fabricating the panels was devised in order to create TCS panels in a cost effective manner for testing purposes. For these reasons, a low-cost fabrication technique was developed at the UTIAS' Multifunctional Structural Lab for this research project. This fabrication technique will be discussed in the following sections.

4.1.1 Quality Control

The quality of a fabricated TCS panel directly affects the accuracy of the test and the correlation to the analytical results. Therefore it is of vital importance that the fabrication technique is accurate and consistent. Various aspects of quality control must be addressed, including truss orientation, truss connection to face-sheets, consistency of core configurations, face-sheet strength, face-sheet weight, flatness of face-sheets, and dimensional control. In terms of truss orientation, the truss or pins must be oriented at a certain angle to the face-sheets according to the design. Depending on the particular TCS design, the pins may have a number of different angles in the unit cell; therefore an alignment method must be capable of providing the versatility to allow the change of the pin angles during fabrication easily. The pins need to be bonded to the face-sheets as rigidly as possible in order to maximize the shear and bending stiffness of the TCS panel. Critically, these properties must be consistent throughout the entire panel.

The quality control issues of the face-sheets will be considered next. Face-sheets are made up of four plies of cross-woven carbon fibre fabrics, which are bonded together by a two-part resin system made up of epoxy and hardener. A wet lay-up procedure is used to fabricate the carbon composite face-sheets. Generally, this involves wetting all the carbon fibre fabrics with the resin, laying them one on top of the other, and a vacuum bagging to extract all the excess resin during the curing process and consolidate the laminate. This process must be carried out properly in order to ensure that the composite has a high strength to weight ratio. In addition, it is important to ensure that the pins are not protruding through the face-sheets. The face-sheets need to be parallel to each other in order to maintain the proper dimensions. Finally, the dimensions of the TCS panel must be correct in order to fit into to the acoustic chamber

window. The thickness of the panel must be properly maintained during the fabrication process, and the length and width of the panel must be at 20-7/8" by 20-3/16". All these quality issues need to be considered and dealt with during the design of the fabrication method.

4.1.2 Fabrication Procedures

In order to maintain the proper dimensions of the TCS panel during the fabrication process, a fixture was built. A sketch of the fixture is shown in Figure 29. In order for the TCS structure to have high shear strength, bending stiffness, and compression stability, the most efficient way to connect the pins to the face-sheet is to insert the pins through the face-sheets. The pins should be inserted through the face-sheets before cure, and due to the large quantity of pins to be inserted into the panel and the relatively short curing time, the pins must be inserted before the carbon fibre cloth is impregnated with resin, which means that the resin can only be applied after the lay-up has been completed. This is not the ideal approach because complete saturation of the carbon fibre cloth can only be ensured if each cloth is wetted individually, and complete saturation will provide maximum strength to the composite. However, this approach is necessary for a manual fabrication method of a large panel. Pressure is applied to the wetted composite in order to ensure complete penetration of the resin.

During the curing process, the orientations of the pins must be maintained between the pair of face-sheets; therefore a layer of polystyrene foam is inserted between the face-sheets before the pins are inserted. The pins penetrate through the top face-sheet, then through the polystyrene foam, and finally through the bottom face-sheet. The foam also has the function of maintaining the proper thickness for the entire panel during the fabrication process, and to stop the resin from leaking to the opposite side of the panel during the two-step curing process. The foam core is removed after the entire panel is completed through chemical dissolution. A pin-guide fixture is created in order to provide the consistency and the accuracy required for the pin angle as a pin is inserted into the pre-cured panel. The pin-guide fixture is shown in Figure 30. It is composed of two layers of perforated board designed to provide the versatility and precision required for all kinds of TCS unit cell designs. Pins are inserted from the top layer of the pin-guide fixture, and depending on the angle of the unit cell design, the pins pass through a specific location on the bottom layer before insertion into the panel. There is an offset between the pin-guide fixture and the surface of the panel so that a cutter can reach the pin and cut off the excess

carbon pultruded rod that is used for the pins. Figure 31 shows that the rods are being cut manually.

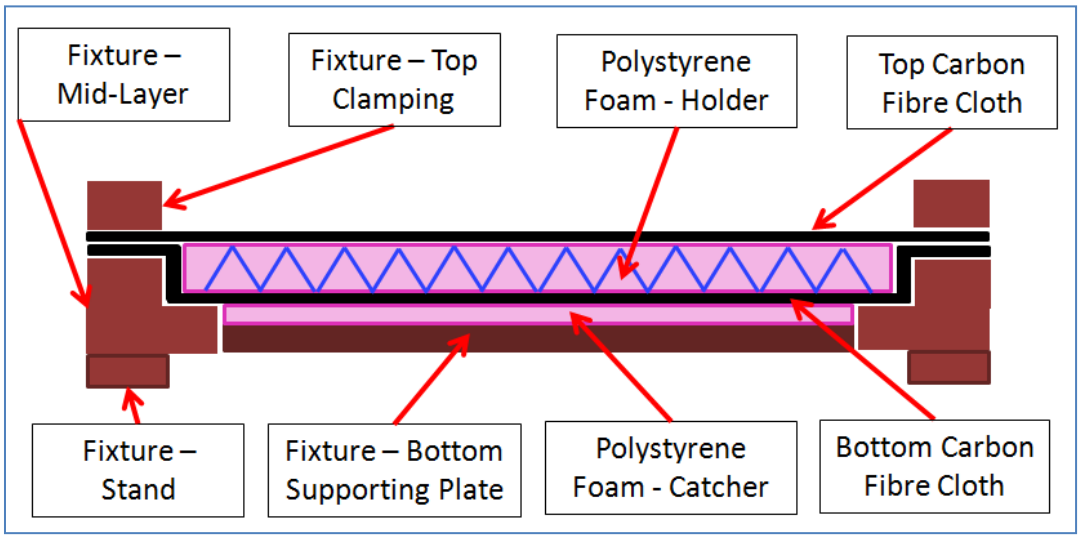

Figure 29. Cross-section of the TCS panel fixture (not to scale)

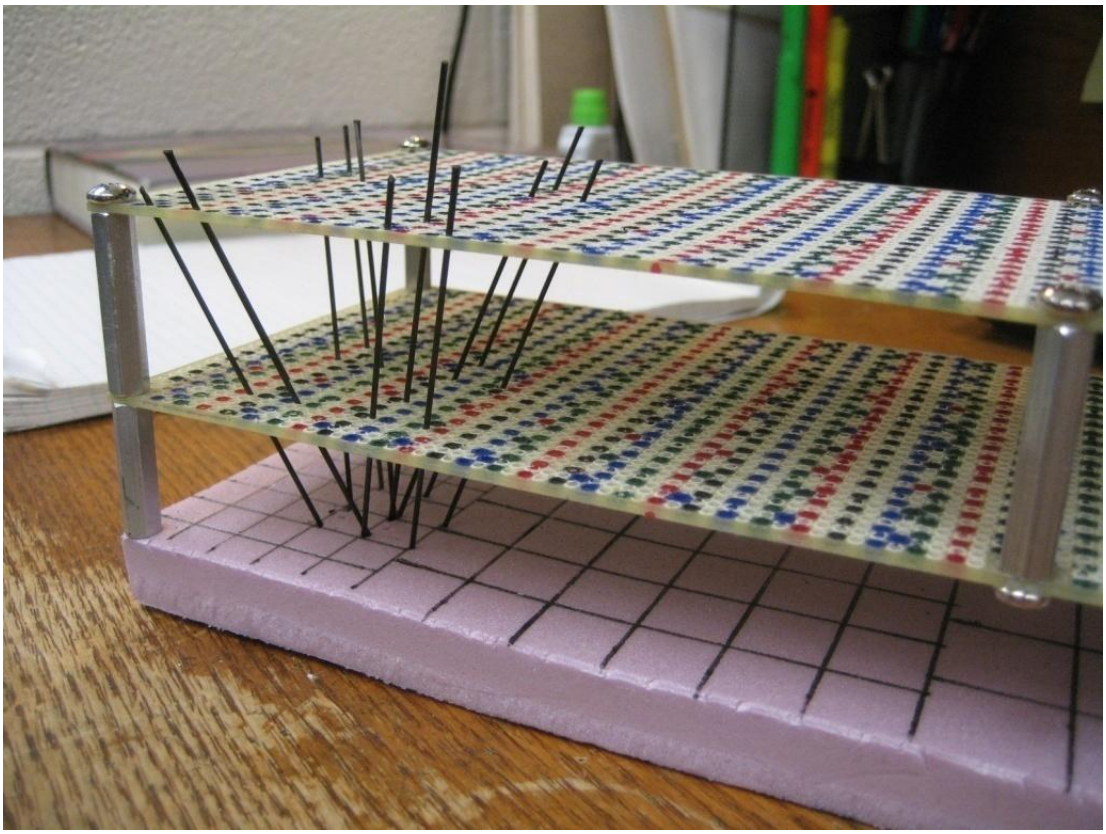

Figure 30. Pin-guide fixture

Three layers of carbon fibre fabric are originally put on top of the polystyrene foam for the pins to penetrate. The fourth layer of carbon fibre cloth is then used to cover the top surface for the purpose of covering the ends of the pins and to add strength to the composite face-sheets.

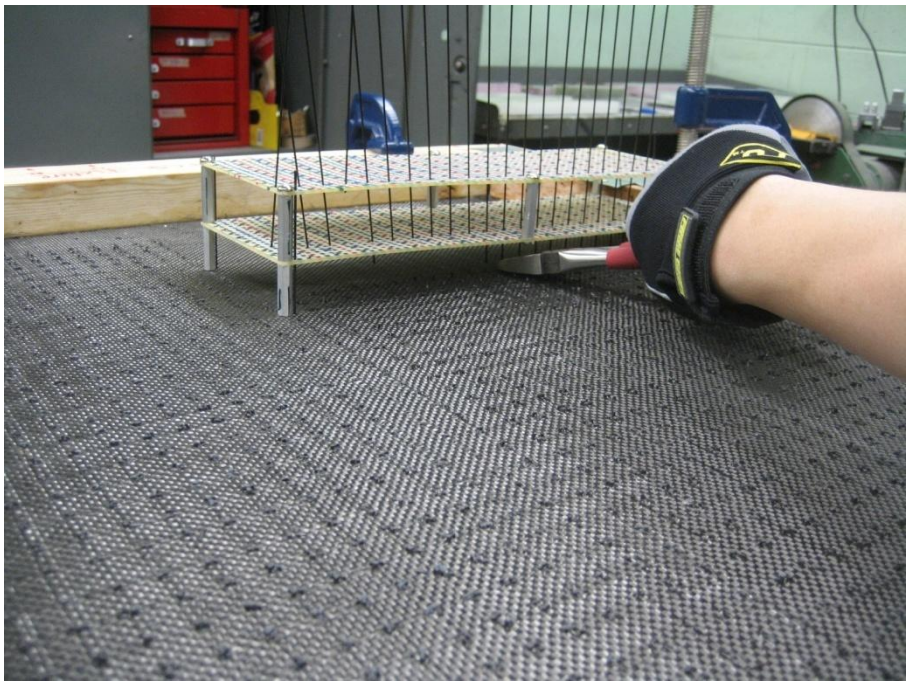

Figure 31. Fabricator cutting carbon pultruded rod

In contrast, four layers of carbon fibre fabric are laid on the bottom when the fixture is set up. This setup can be seen in Figure 32 and 33. Note that there is a layer of thin polystyrene foam between the bottom layer carbon fibre fabric and the hard surface of the fixture. It is in place because the soft layer of foam will make sure that the pins can be penetrated through the bottom layer, and it also helps to secure the pin ends during the fabrication process. This is shown in Figure 34. The pins are inserted from the top of the panel and they are stopped by the bottom supporting plate. It should be noted that the ends of the pins are cut with a sharp angle to improve the penetration performance, as shown in Figure 35. After all the pins are inserted, the bottom supporting plate is removed to allow the excess carbon rods on top of the panel to be pushed further into the panel before the final carbon fibre fabric is laid on the panel. This process is shown in Figure 36. This will ensure that the ends of the pin will not protrude from the panel after curing.

Figure 32. TCS panel fixture – showing the bottom carbon fibre sheet lay-up

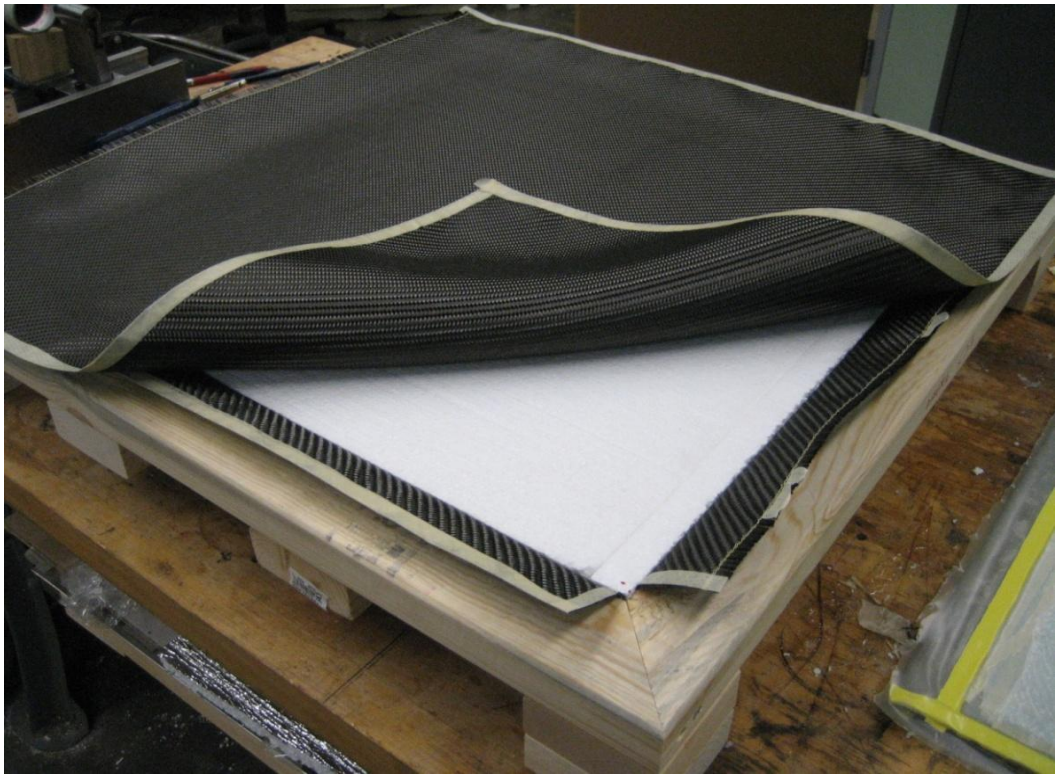

Figure 33. TCS panel fixture – showing the bottom carbon fibre sheet lay-up

A two-part curing process was used to cure the panel. The top side of the panel was cured first, followed by the bottom side of the panel, which will be cured in a separate step. Resin was applied to the sheets on the top side of the panel. The top side was then covered by a layer of peel-ply, then a breather-ply, followed by a half-inch particle board, and finally a cover sheet for vacuum bagging. The half-inch particle board provided a uniform flat surface to the panel during the curing process. If it was not in place, the pressure of the vacuum bag pushed the carbon fibre fabric into the supporting foam core, causing the pins to protrude out from the face sheet. A vacuum pump removed the excess resin in the impregnated carbon fibre cloth. Due to the large surface area of the panel, two access points are used by the vacuum pump, one at each opposing corner of the panel, to remove the excess resin effectively. This process is shown in Figure 37. It is advised that the package, which contains the TCS structure wrapped by a vacuum bag, be turned upside-down in order to prevent excess resin from entering into the foam core. After the top layer is properly cured in twenty- four hours time, the bottom layer can be processed. The protruded pins on the bottom surface are cut using a rotary cutter. Care should be taken when cutting the protruded ends since the carbon fibre fabric may be damaged

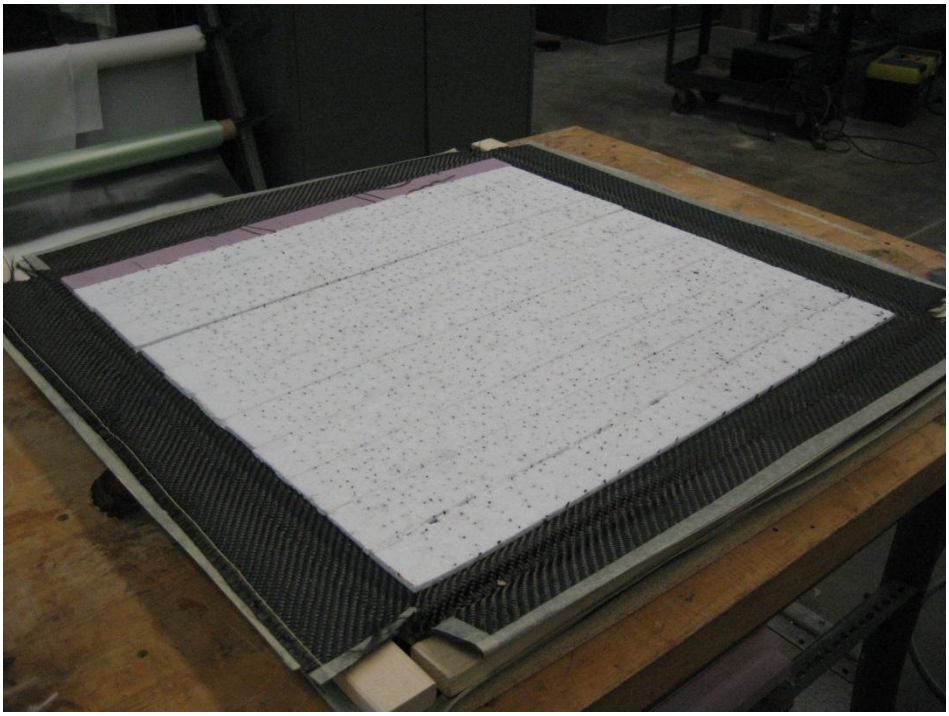

Figure 34. TCS panel fixture – showing bottom catcher polystyrene foam – after the pins are inserted

Figure 35. Carbon pultruded rod is trimmed to improve penetration performance

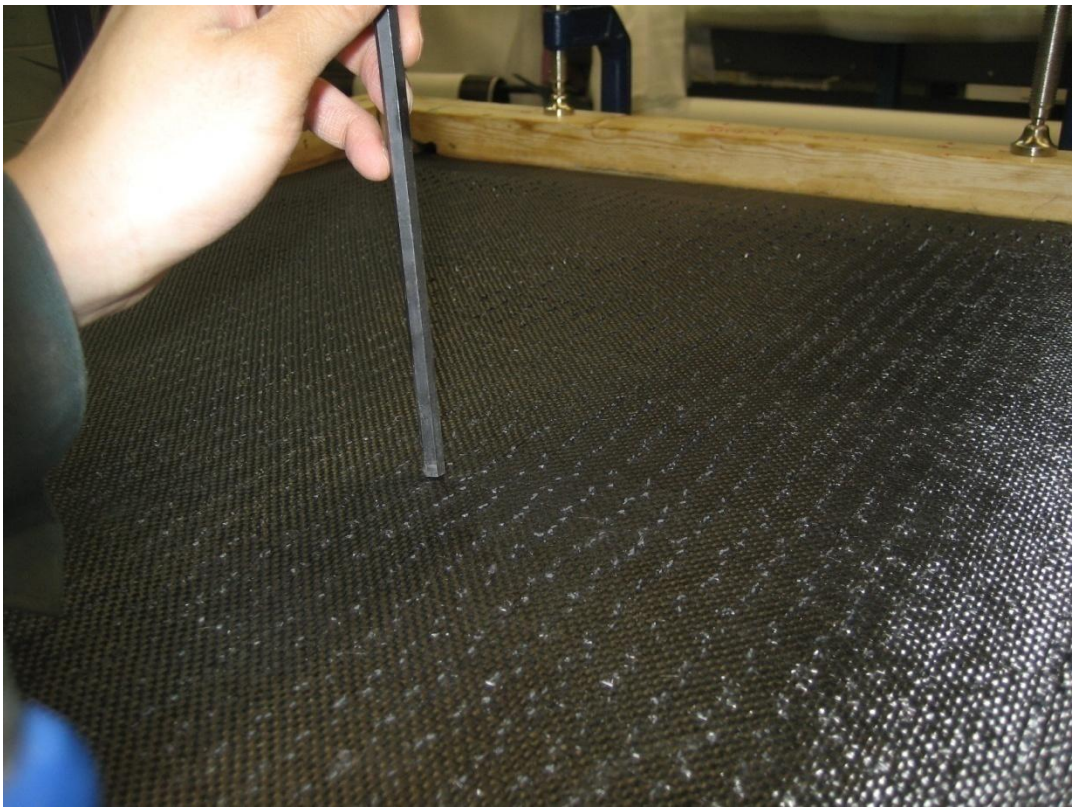

Figure 36. Pins being pushed further into the core to ensure smooth surface

during the operation. Resin is then applied to the bottom surface of the panel to create the carbon composite face sheet. Similar procedures as the top face-sheet are used in curing the bottom face sheet. After both the top and the bottom surfaces of the TCS panel were cured, the

panel was cut into the dimensions for testing in the acoustic chamber. The next step was the removal of the foam core using acetone. Previous experiments showed that acetone will not reduce the strength of the carbon composite and the carbon pultruded rod when they are submerged into the solution for less than one hour. A tub was built and the TCS panel was submerged into the wooden tub, which was filled with acetone. The tub was lined by high-strength plastic sheet before acetone was used to fill the tub. The final product is shown in Figure 38.

Figure 37. Vacuum bagging of the TCS panel

Two TCS panels were constructed for testing at the Bombardier Aerospace's acoustic chamber. The first TCS panel has a tetrahedral unit cell design and the second panel has a pyramidal unit cell design. The tetrahedral and pyramidal unit cell design TCS panel have the average thicknesses of 1.6 cm and 1.8 cm respectively. The difference in thickness is caused by the vacuum bagging process when one panel is being compressed more than the other. The weight of the panels are 1.106 kg and 1.474 kg, the corresponding panel densities are 0.226 g/cm^3 and 0.301 g/cm^3, and the areal densities are 0.361 g/cm^2 and 0.542 g/cm^2 for the tetrahedral and the pyramid unit cell design TCS panel respectively. The difference in weight is due to the difference in unit cell design and the mixture of residual foam and cured resin that is left in the structure. The tetrahedral unit cell structure allows the foam to be removed more easily than the pyramid unit cell design, and, consequently, the pyramidal unit cell design TCS

panel has more residual foam and hence the weight is increased. This is unavoidable using the current manual fabrication techniques.

Figure 38. Complete TCS panel – tetrahedral unit cell TCS panel

4.2 Acoustic Chamber Testing of TCS Panels

The acoustic chamber experiments were carried out at the Bombardier Aerospace acoustic lab. The stand-alone, mid-size acoustic chamber is used for these experiments. In the following sections, the experimental setup and the experiment results will be discussed in details.

4.2.1 Incident Sound Field

The general acoustic chamber test set-up is shown in Figure 29. White noise is used as the sound source, and it is created by the speaker inside the acoustic chamber. In order to ensure that a diffused sound field is developed at the incident surface of the TCS panel, four microphones, each located in different point in space, were used to measure and validate the incident sound field inside the acoustic chamber. An example of the spectrums and intensities of the incident sound field measured by the microphones are shown in Figure 39. The average standard deviation of all the tests is approximately 1.66, which shows a high degree of diffusivity in the incident sound field. Since white noise is used in the experiment, a means to discretize the continuous sound spectrum is required to measure the spectrum intensity of the sound field. For

this reason, the continuous sound spectrum needs to be split into octave bands. One-third octave band is used in this experiment in order to provide a more detailed description of the frequency content of the white noise.

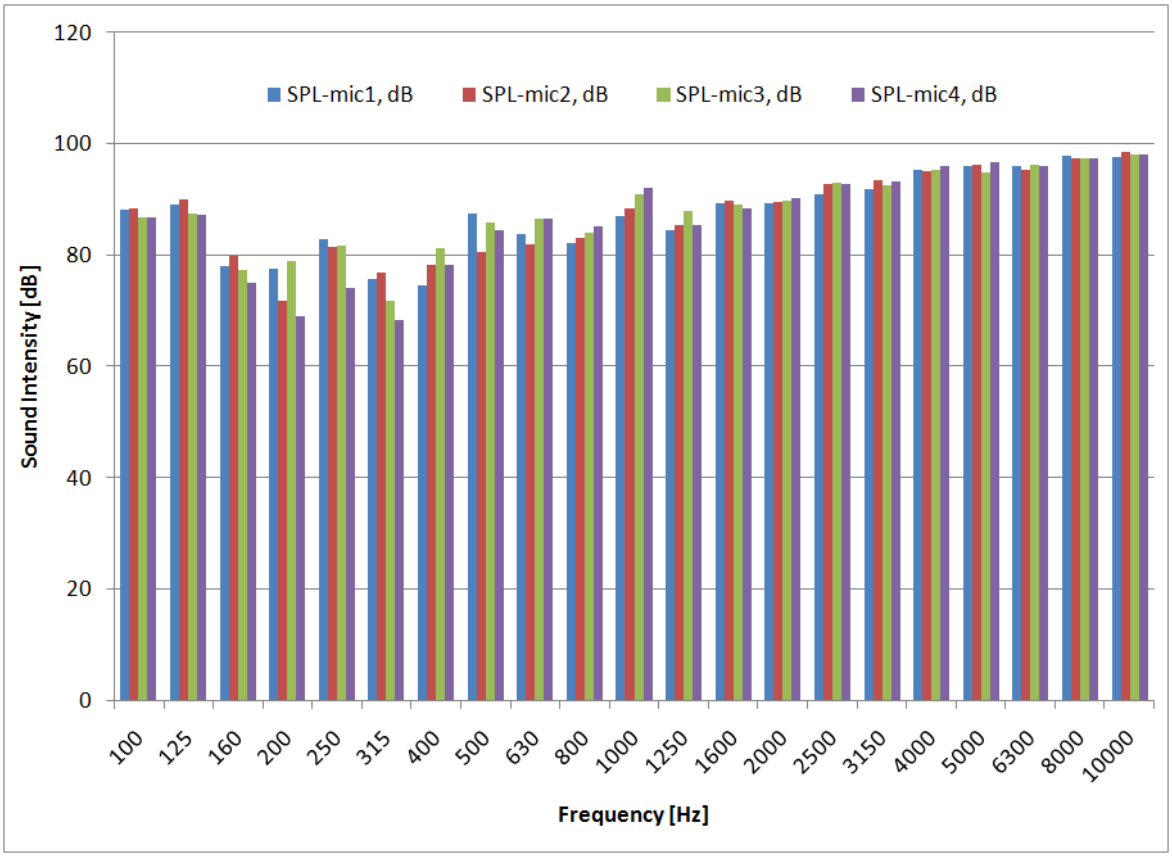

Figure 39. White noise incident sound field spectrum intensity

4.2.2 TCS Panel Installation

A TCS panel is installed at the acoustic chamber window using a silicone based polymer to provide the required adhesion and damping properties at the boundaries. There is a 2 mm gap between the acoustic chamber window and the TCS panel perimeter. The gap is in place in order to reduce the acoustic chamber‘s structural vibration load on the TCS panel. Note that due to the size of the acoustic chamber, the vibration of the panel is coupled with the acoustic chamber under approximately 800 Hz. Thus, the data between 100 Hz to 800 Hz contains noise and should not be used for the analysis.

4.2.3 Data Acquisition and Processing

A sound intensity probe is used to measure the response of the panel to the incident sound field. The sound intensity probe measures the velocity of the particles in the medium, hence the pressure fluctuation and the sound intensity spectrum in the medium can be determined. The probe measures the sound intensity at approximately 2 inches from the transmitting side of a TCS panel. The sound intensity probe has been calibrated by Bombardier Aerospace personnel according to the probe manufacturer's standard. Each of the two panels being tested was scanned three times. The probe was moved by an operator in the horizontal pattern and the vertical pattern, as shown in Figure 40, at a constant speed in order to determine the average sound intensity level radiated by the TCS panel. The horizontal pattern was used two times, and the vertical pattern was used one time in each experiment. The sound intensity level was measured in decibel (dB) at each one-third octave frequency. During each test, the average of the three scans was used to determine the performance of a TCS panel.

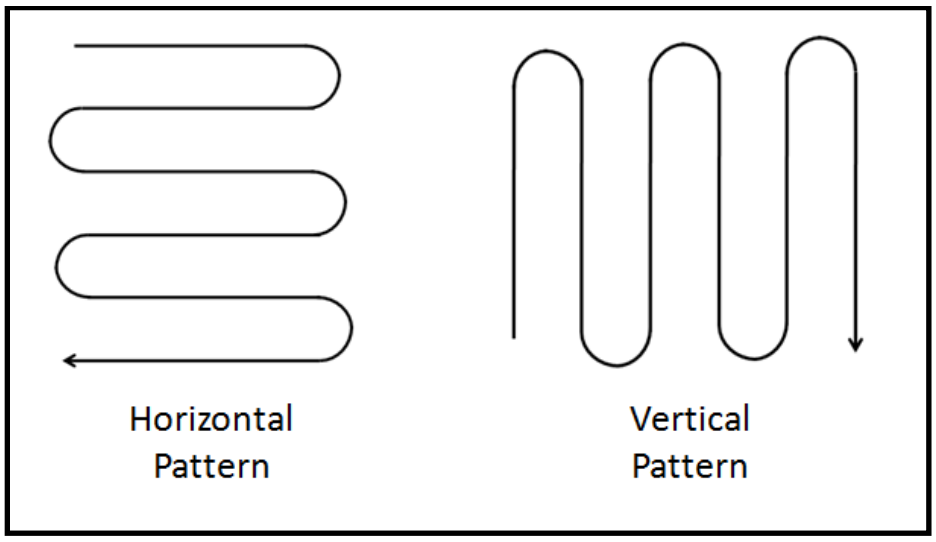

Figure 40. Sound intensity probe scanning pattern

The unit used for the sound intensity measurement results is in decibel with a reference pressure of 2e-5 Pa. The Intensity or sound intensity level (SPL) can be calculated by:

$$SPL = 20 \cdot log_{10}\left(\frac{P}{P_0}\right), \tag{4.1}$$

where P is the sound pressure, and P_0 is the reference pressure. The transmission loss (TL) of a panel describes the effectiveness of a panel to reduce noise being transmitted through a panel, which is defined as:

$$TL = 10 \cdot log_{10}\left(\frac{I_T}{I_I}\right), \tag{4.2}$$

where I_T is the transmitted power, and I_I is the incident power. The results of the acoustic chamber tests of the two TCS panels in terms of TL are shown in Figure 41. The results clearly showed that the pyramidal unit cell design is more efficient in reducing the noise transmitted through the TCS panel than the tetrahedral unit cell design across the entire frequency range of interest.

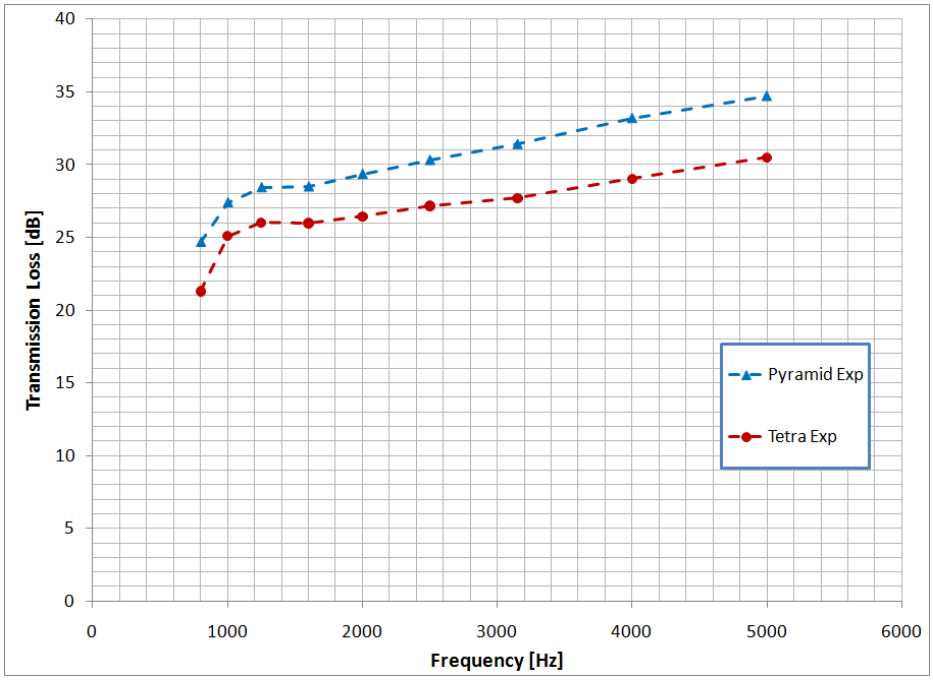

Figure 41. Acoustic chamber test results for two TCS panel in terms of transmission loss

4.3 Comparison to the Finite Element Analysis Results

In order to compare the FEA results with the experimental results, the results of the FEA were converted into TL values using the formula developed in [27]:

$$I_{rms} = 20 \cdot log_{10}\left(\frac{v_{rms}}{v_0}\right), \tag{4.3}$$

where I_{rms} is the intensity in dB, v_{rms} is the root-mean-squared velocity of the panel, and v_0 is the reference velocity, which is equal to 5e-8 m/s. The resulting TL values for the two TCS beam structures in the frequency range of interest are shown in Figure 42. Note that the results have been normalized using the experimental results in order to compare the performance in both the experimental and FEA cases on the same graph. It should be emphasized that the FEA model is a beam structure with a specific unit cell design, and the experiments are carried out using a TCS panel structure. The beam structure has the same length and thickness as the panel structure, but the width of the beam structure only represents the width of one row of unit cells in a panel structure. Hence the boundary conditions of the beam structure only correspond to the panel structure in the length-wise direction, but not in the width-wise direction.

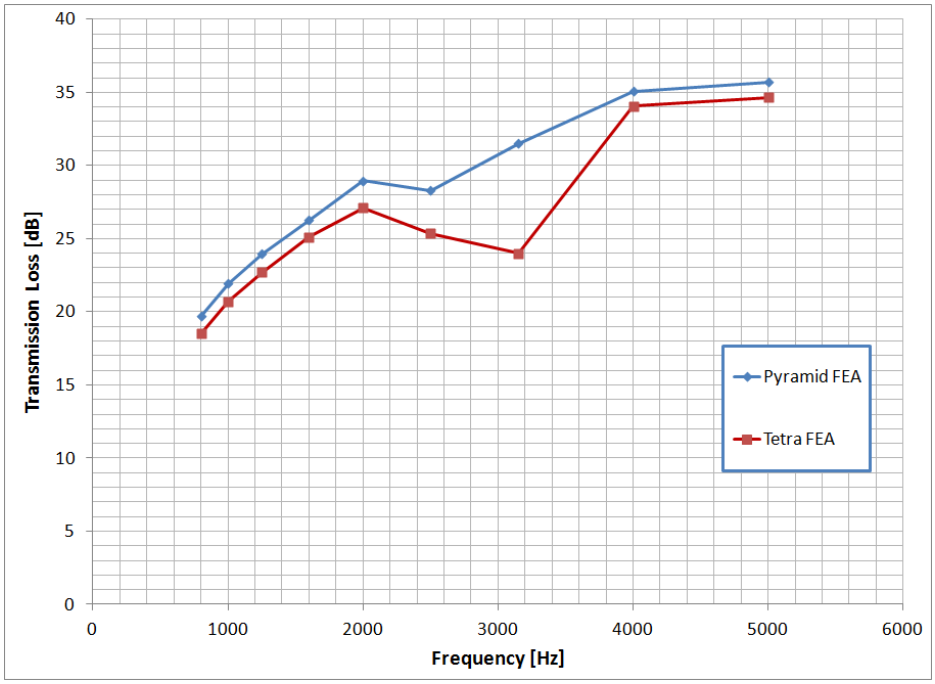

Figure 42. Normalized finite element analysis result for two TCS panels' responses under unit pressure load in terms of transmission loss

4.4 Discussions

The results of the experiments clearly show that there are significant differences in the acoustic performance between the pyramidal unit cell TCS panel and the tetrahedral unit cell TCS panel. The average transmission loss difference between the two panel designs is approximately 12%. Similar trends are also observed in the FEA models, however the difference is only around 9% with the pyramid unit cell design structure having a higher TL. The difference between the FEA and the experimental results may be caused by the difference in boundary conditions, mass, and damping characteristics. Although a direct comparison cannot be made between a beam structure and a panel structure, the difference in performance between the two TCS structures is similar because the same mechanisms are involved in producing the transmission loss in both structures. One major difference between the two structures is the difference in boundary conditions. The beam structure only closely resembles what the center strip of a panel experiences under an acoustic load; it is not representative of other parts of the panel. As a result, the absolute TL predicted by the FEA results should not be used to correlate to the experimental results. Another difference between the FEA and experimental results is the mass. The actual pyramid unit cell design TCS panel weights 25% more than the tetrahedral unit cell design, however the FEA model only shows a 1.1% difference in mass. As explained in section 4.1 of this chapter, the difference in mass is mainly caused by the mixture of residual foam and cured resin left in the panel after the foam core is removed by chemical erosion. The normal incidence mass law stated that the mass of a panel only has significant effect on the TL properties when the excitation frequency is well above the natural frequency. This is shown in the following relationship. For $\omega \gg \omega_0$:

$$TL \propto log_{10}(mf), \tag{4.4}$$

where ω is the excitation frequency, ω_0 is the natural frequency of a panel, m is the mass of a panel, and f is the excitation frequency in hertz. Therefore, the higher the mass, the higher the TL will be at a frequency well above a natural frequency. This may be used to explain the larger difference in TL between the pyramid and tetrahedral unit cell design panels in the experiment than the FEA results. It should be noted that the tetrahedral unit cell design beam structure reaches a resonance value at around 3000 Hz (See Figure 19a). This is observed in the FEA results in Figure 43, where the TL of the tetrahedral beam drops significantly at 3150 Hz. In the

experiments, this drop in TL is not observed, and this may be due to damping. The FEA models were idealized by only considering their undamped characteristics, therefore the resonant responses are prominent. However, the TCS panels fabricated for the experiments have a substantial amount of polystyrene foam deposited on the surfaces of the carbon pultruded rods, and they act as a damping material, dissipating the energy associated with the structural vibration. As the result, the experimental results are expected to be fairly uniform, with low sensitivity to the resonant frequencies found in the idealized structures.

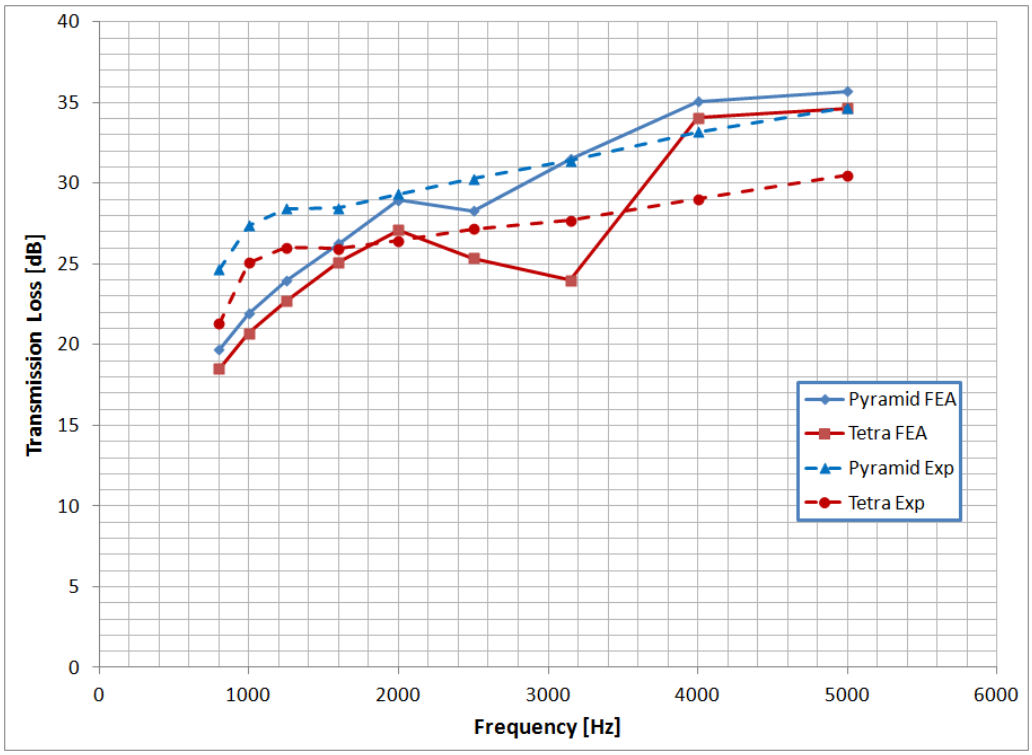

Figure 43. Comparison of experimental and normalized FEA results of two TCS structures' transmission loss characteristics

Despite the various factors that cause the difference between the FEA and the experiment results, the FEA correctly determined the trend of the performance between the two TCS unit cell designs. Figure 44 shows the experimental and the normalized FEA results on a single graph for comparison. This demonstrates that by properly designing the unit cell structure for a TCS panel using the guidelines and the analytical methods outlined in this report, one can obtain a TCS panel design with superior acoustic and other structural properties. The results from the experiment also highlight an important characteristic of TCS structure, which is the influence of the unit cell design to the overall acoustic performance. If all the foam at the core were removed,

the difference in weight between the two panels should approach the theoretical value, which is around 1.1%. Thus, a design having only 1.1% difference in weights, can have as much as 9 % difference in acoustic performance. Along with the other advantages offer by TCS structure, it is concluded that TCS structure provides a plausible solution to control the noise inside an aircraft cabin.

Chapter 5

Discussion

In order to develop a set of design guidelines and analysis methodologies for designing TCS panels for reduction of cabin acoustic noise, several analysis techniques were used and experiments were performed. This demonstrated the appropriateness of using these analyses for design purposes. A review of the literature showed a lack of research into analyzing TCS structures at the component level for noise reduction applications. Therefore, the current research is intended to fill this gap. In order to achieve this research goal, theoretical analyses were first carried out, followed by numerical simulations, and finally acoustic chamber experiments were performed.

The dominant acoustic noise in an aircraft cabin is caused by the turbulent boundary layer (TBL) induced pressure fluctuation, which causes vibration of the aircraft panels, radiating sound into the cabin. Analyses showed that the radiated sound level and the transmission loss properties of interior aircraft panels are related to the root-mean-squared (RMS) velocity of their surfaces, as discussed in Section 2.1.2, and shown in Equation [2.10]. Therefore an evaluation of the vibration characteristics of these structures will reveal their acoustic performance. In order to reduce the computational cost of the analyses, a TCS beam structure was analyzed instead of a panel structure. A normally incident time-harmonic pressure load was used as the forcing condition, and the beam had a simply supported boundary conditions. The frequency range under consideration in this research was between 20 Hz to 4000 Hz, which represents the most important frequency range for the specific application of cabin noise reduction on a commercial aircraft. It was found that 15 points, evenly distributed along the length of a beam, were adequate to represent the frequency response of the beam under a harmonic pressure load.

The results from the analytical frequency response analysis correlate well with the initial FEA results. Analytical results showed that a beam will have higher natural frequencies corresponding to higher Young's modulus and shear modulus, as well as lower density and shorter length. While the relationships between the excitation frequencies and most of these parameters are similar at different modes, only the shear modulus has different relationships with the excitation frequencies at different modes (See Figure 14). This characteristic allows the natural frequencies of a specific vibration mode to be altered by modifying the shear modulus. The Young's modulus and the shear modulus are related through the following relationship in a homogeneous material:

$$G = \frac{E}{2 \cdot (1 + \upsilon)}, \tag{5.1}$$

where G is the shear modulus, E is the Young's modulus, and υ is the poisson's ratio. Even for an inhomogeneous material, the shear modulus is still strongly coupled with the Young's modulus. Therefore, it may be challenging to alter the shear modulus of a material without affecting the Young's modulus. However, it is advantageous for acoustic control purposes to be able to manipulate the tensile stiffness and the shear stiffness of a sandwich structure separately due to the relationships between bending waves, shear waves, and transmission loss (TL).

Bending waves are the main mechanism that drives out-of-plane motion in a panel when it is excited, and they provide the adjacent air particles in the medium with sufficient velocity to cause sound radiation from the panel. Due to the nature of the bending (flexural) wave propagation in a solid, the governing equation for bending wave is a fourth order differential equation, and the velocity of flexural wave is a function of the frequency of propagation. This phase velocity is proportional to the square root of the frequency; hence bending waves in solid are dispersive. Unlike bending waves, shear (transverse) waves show no dispersion, and therefore the shear wave phase velocity is not a function of frequency. When the wave speed exceeds the speed of sound in the medium, the interaction between the panel and the medium becomes efficient, and transmission loss of the panel will decrease. Since the propagation velocity of the bending wave is proportional to the square root of frequency, therefore it is a monotonically increasing function of frequency, which indicates that there is always a frequency above which the bending wave speed exceeds the speed of sound in the medium and hence sound

radiation becomes efficient. If a panel is constructed in such a way that it favors the propagation of shear waves rather than bending waves, such panels would have good transmission loss properties if the designed shear wave speed is less than the speed of sound in the medium. It is impossible to achieve this design criterion in a homogeneous panel due to the fact that bending stiffness is directly proportional to shear stiffness in a solid. However, a sandwich panel may be able to provide high bending stiffness for structural purposes, and low shear stiffness for acoustic purposes. In practice, if the core of a sandwich structure is made of a soft but incompressible core, such as rubber, and the face-sheets are made of high stiffness material, such as carbon fibre composite, the aforementioned design objective can be achieved. Bending of such panels would cause tensile and compressive stress on the top and bottom face-sheets respectively, whereas shear deformation of the panel would require shear of the core material. Therefore, such panels will be stiffer in bending than in shear, and shear waves may be the dominant propagation waves in the panel due to the thickness and mass of the core. Since the bending stiffness of a TCS panel is mainly controlled by the face-sheets and the distance between them, and the shear stiffness depends on the configuration of the pins and their mechanical connections to the face-sheets, bending and shear stiffness of a TCS panel may be individually controlled with reduced coupling between.

On the other hand, Moore and Lyon [25] suggested another design approach may be suitable for designing TCS panels. Their design acts as a band pass filter, which provides a high transmission loss at the frequency band of interest. This can be achieved by moving the double wall resonance frequency to occur below the frequency band of interest, and the core shear stiffness is carefully controlled so that coincidence for antisymmetric motion is delayed and occurs above the band of interest. A double wall resonance occurs when symmetrical mode resonance takes place, which causes the face-sheets to move in the opposite directions, hence resulting in a change in panel thickness. In contrast, anti-symmetric panel motions occur when both face-sheets move in the same direction therefore no thickness change occurs in the panel. Using a low compressional stiffness and a high shear stiffness core, the symmetric and antisymmetric motions of the face sheets cancel out and produce a transmission loss higher than the mass law.

Depending on the application and the operation environment, the designer needs to determine which design approach to use. The two approaches take advantage of the fact that the

compressional and the shear stiffness of a sandwich structure can be manipulated separately to attain a certain sound insulation effect at a given frequency range. Therefore, it is important to determine if TCS structures would allow this characteristic to occur, and the degree of uncoupled behavior. This would allow designers to use various design schemes, such as wave propagation characteristics, impedance control, vibration interference, etc, to tailor the acoustic properties of a TCS structure to achieve a high level of transmission loss.

Finite element analyses were performed in order to achieve this goal by investigating the interaction between various TCS designs and their responses to acoustic type loads. Four different unit cell designs were used to investigate the various relationships between the design parameters and the vibro-acoustic responses. These four unit cell designs are Kagome, pyramidal, tetrahedral, and diagonal array unit cell designs. Note that it is beneficial for TCS panel design to have low modal density, and low response magnitude, because lower modal density allows the engineers to have more design room to avoid coincidence with the forcing frequencies, and lower response magnitude means lower cabin noise level. The FEA results indicated that different unit cells have significantly different response magnitudes and modal densities. In addition to changing the unit cell designs, changing the core pin diameter can also change the modal density. As well, changing the pin diameters can also slightly increase the first resonant frequency, and significantly change the second resonant frequency. Increasing the face-sheet thickness has the effect of lowering the response magnitude.

It was found that the Kagome unit cell design provides the highest effective bending and shear stiffness compared to the other unit cell designs from the static FEA analyses. The effective bending stiffness of a beam is the major parameter that controls the first resonant frequency, and therefore the overall beam dimensions and the unit cell designs provides the best tool to control it. The bending stiffness of a beam is related to its moment of inertia, which is strongly related to the thickness of a beam. The thickness and the length of a beam vary by the power of three and four respectively with the natural frequency of a beam, and therefore varying the dimensions of a beam has a significant effect on its bending stiffness and the first resonance frequency. This can be observed in Equations [2.34] to [2.37]. At higher modes, other details of a beam, such as core design and damping, play an increase role in determining the natural frequencies. After the Kagome unit cell design, the pyramid unit cell design provides the second highest bending and shear stiffness. However, while the Young's modulus, which is related to

the bending stiffness of the TCS beam, of the Kagome unit cell design is approximately 2.5% higher than the pyramid unit cell design, the shear modulus of the former is 59% higher than the latter. As a result, the modal density of the pyramid unit cell design is higher than the Kagome unit cell design in the mid frequency range. This can be seen in Figure 19a. This highlights the importance of unit cell design on the structural as well as the acoustic characteristics of TCS structure. On the other hand, when comparing the pyramidal and the array unit cell design, it was found that the bending stiffness of the pyramidal unit cell design beam is approximately six times higher than the array unit cell design TCS beam, however the shear stiffness of the former is only 1.4 times higher than the latter. This unit cell design analysis indicates that by spatially separating the connection points between the pins and the upper face-sheet, the shear stiffness tend to increase more than the effective bending stiffness. In the pyramidal and tetrahedral unit cell design, the pins are connected to the same point at the upper face-sheet, however for the array and Kagome unit cell designs, the pins are connected to the upper face-sheet in different locations. Note that the shear stiffness for these beam structures was measured in the longitudinal direction only. Due to the orthotropic nature of the array unit cell design, it is expected that the span-wise shear modulus is smaller than the reported length-wise value. It should be emphasized that it is beam structures that are being analysed in the FEA, not a panel structure. The behavior of a beam structure will provide important characteristic trends of a TCS panel structure. This will be shown in the correlation between the FEA and the experimental results in the last section of this chapter.

One of the design parameters that can change the bending and shear stiffness properties of a TCS structure is the pin angle. In order to explore the effect of pin angle on the acoustic and structural response, two TCS unit cell designs were analysed and compared. They were the original array unit cell design, which has a pin angle of 56°, and a modified array unit cell design, which has a pin angle of 45° from the bottom face-sheet. The static analyses showed that while the bending stiffness was slightly increased in the modified array unit cell design TCS beam, the shear stiffness was significantly improved when the pin angle was dropped by 11°. This large increase in shear stiffness shows that pin angle has a strong influence on a TCS structure's shear properties if the pin is oriented in the direction of the measurement. As mentioned above, the shear stiffness is only measured in the length-wise direction. A panel with similar unit cell design is not expected to have such a high shear stiffness due to the orthotropic

nature of the unit cell design. Despite the large difference in the effective shear modulus of the two designs, the natural frequency of the first mode is nearly identical. This shows that the low frequency modes depend strongly on the effective bending stiffness of the structure but not on the shear stiffness. The low bending stiffness of the array design cause the natural frequency to be 1.6 times lower than the Kagome unit cell design. Although the bending and shear stiffness characteristics of the whole panels were analyzed, the component level – face-sheets and core, characteristics are not well defined. This is because in a TCS structure, the core is made up of pins positioned and locked in place by the face-sheets, and therefore it is not a standalone component in the structure. This connectivity between the core and the face-sheets introduces difficulties in component level analysis. The modal frequency is similar in both cases, even though the mid resonant frequencies are different between the two designs. In addition, the modified array unit cell design, which has a lower pin angle, has a higher first resonance frequency – approximately 7.9% higher than the original design. This represents a moderate increase in the first mode characteristics. Comparing the array unit cell design to other unit cell designs, the array unit cell design has a significant reduction in the first resonant frequency. The pyramidal, Kagome, and tetrahedral unit cell design TCS beams' first resonant frequencies are 161%, 165%, and 136% higher than the array unit cell design, while the areal densities of all designs are similar. This again shows the significance of unit cell designs on the acoustic behavior of a TCS beam. One of the reasons that the array unit cell design has a lower first resonant frequency and bending stiffness is because the pins are only capable of carrying load in two of the three principal directions. Introducing a pin that carries the acoustic vibration load on the cross-section plane (*yz*-plane) may increase the unit cell first resonant frequency and bending stiffness.

Another design parameter that can be tailored in order to control the acoustic properties of a TCS structure is the spatial distribution of the unit cells. This design parameter can be easily adjusted in practice for a TCS structure, and therefore it is one of the unique characteristics of such structures. Three models were analyzed using FEA in order to determine the effect of unit cell spatial distribution. The tetrahedral unit cell design was used as the baseline design for comparison. Two alternative designs with one having an increased distance between the adjacent unit cells (design [6]), and the other one having a decreased distance between the adjacent unit cells (design [7]) were used in this study. The bending stiffness of design [6], which has a high pin density at the boundary, is comparable to the original tetrahedral unit cell

design TCS beam, however design [7] has a bending stiffness which is approximately 27% lower than the original design. This shows that the bending stiffness of a TCS beam structure is sensitive to the pin density at the support, and it tends to decrease as the local pin density is decreased. The effective bending stiffness of design [6] is similar to the original tetrahedral unit design, which resulted in a comparable first resonant frequency, however the resonant frequencies in the mid frequency range is considerably lowered. Both alternative designs showed lower resonant frequency across all frequency ranges than the original design. This phenomenon is mainly due to the lowering of the local bending stiffness at either the ends or the center of the beam. The FEA results indicated that the overall bending stiffness only has a dominant effect on the first mode, and the stiffness distribution has more significant effects on the resonant frequencies in the mid frequency range. From the static analysis, it was observed that the overall effective bending stiffness of design [6] was decreased by 3% while the overall effective shear stiffness were increased by 90% compared to the original tetrahedral unit cell design TCS beam. Note that these values only represent average values of the entire beams, while the local values along the length of the beams may be different. The significance of altering the spatial distance between the unit cells, hence the stiffness distribution, is related to shifting the resonant frequencies of a beam and the relative changes between the bending and shear stiffness. This provides the designer another important tool to tailor the acoustic properties of TCS structures.

Core mass is another important design parameter that may provide designers a means to customize a TCS structure's acoustic and structural properties. In order to investigate this phenomenon, a model with a higher core mass was analyzed by FEA, and the result was compared to other designs. By increasing the pin density, the core mass of a TCS structure was increased. Using the tetrahedral unit cell design as the base structure, the core mass was increased by approximately 40% so that it matched the core mass of the pyramid unit cell design. This comparison provides another insight into the relationship between unit cell design, stiffness, and mass of TCS structures. The modified tetrahedral unit cell design TCS beam with increased core mass (design [8]) has a lower bending stiffness, lower frequency for the first mode, similar transmission loss value, and the same shear stiffness as the original tetrahedral unit cell design. The core mass is only a small percentage of the overall mass – 3.91% and 2.83% for the pyramid and the original tetrahedral unit cell design respectively, therefore the effect of the pin density does not have a large effect on the structural and acoustic properties of the TCS beams. By

comparing the pyramid and the modified tetrahedral unit cell designs, it can be concluded that unit cell design has a larger influence on the structural and acoustic properties of a TCS structure than the core mass. This is shown in Figure 23.

The parameters associated with the face-sheets of a TCS structure can also be tailored in order to control the structural and acoustic properties of the whole structure. By increasing the density of the face-sheets, the mass of the face-sheet is modified in design [9], which uses the tetrahedral unit cell design. The face-sheets of design [9] have twice the density of the baseline tetrahedral unit cell design, while the density of the pins is unchanged. Both the bending and shear stiffness are the same in both designs, namely design [3] and [9]. However, the frequency of the first mode for design [9] is approximately 29% lower than the original design with lighter face-sheets. In addition, all the subsequent modes occur at lower frequencies. This may or may not be desirable for acoustic purposes, depending on the design scheme and the operation conditions. The average transmission loss values for the various designs are shown in Table 7. Note that the average values are for reference only because the actual acoustic performance is a function of the excitation frequency, which is not evident in the average values. The transmission loss of design [9] is 18.2% higher than the same unit cell design TCS beam with lighter face-sheets, while the mass is 49.3% higher. This trend agrees with the normal incidence mass law, which states that if the medium is air, for a homogeneous partition, the transmission loss, mass, and frequency are related by:

$$TL = 20 \cdot log_{10}(mf) - 42\ dB\ , \tag{5.2}$$

where *TL* is the transmission loss of the partition, m is the mass per unit area, and f is the excitation frequency. The mass law shows that the transmission loss increases with mass, which correspond to the results observed from the FEA. The mass law predicts that the transmission loss is increased by 5.9 dB, and the transmission loss predicted by FEA is 5.4 dB, which represents only an 8% variation; therefore the mass law is a good prediction of the FEA results despite the fact that the mass law is derived for homogeneous materials.

Another design parameter associated with the face-sheet design is its thickness. Two additional finite element models were used to investigate the effect of face-sheet thickness. Design [10] and Design [11] use the tetrahedral unit cell design as their core, and their face-sheet thicknesses are 4mm and 1mm respectively. The bending stiffness of the TCS beam design with

thicker face-sheets increased by 68.5%, whereas the one with thinner face-sheets was decreased by 49.7%. Note that the mass of the thicker face-sheet model is the same as design [9], which has double the mass of the original tetrahedral unit cell design. The shear stiffness of design [10] also increased, by 40%, and the shear stiffness of design [11] decreased by 39.4%. Unlike the changing only the density of the face-sheets, changing the thickness of the face-sheets changes the stiffness and the mass of the system, hence both the structural and acoustic behavior of design [10] and [11] are altered. The transmission loss of design [11] was decreased by 17.2% and it is increased by 18.4% in design [10] when compared to the baseline design (design [3]). Comparing the transmission loss values of design [9] and [10], one can observe that the effect of

Design	Unit Cell Design	Young's Modulus E [GPa]	Shear Modulus Gx [MPa]	Average TL [dB]
1	Pyramid	85.89699	241.588	25.59699
2	Kagome	88.01811	384.098	25.70475
3	Tetrahedral	69.21273	45.425	24.01689
4	Array	12.33716	99.697	25.30839
5	Array 45° pin angle	14.42024	487.630	25.55513
6	Tetra packed edge	67.14329	86.182	22.20573
7	Tetra packed center	50.71594	75.874	24.7419
8	Tetra heavy pin	65.15213	45.425	24.12016
9	Tetra heavy face-sheet	69.21273	45.425	29.38775
10	Tetra thick face-sheet	57.27784	61.761	29.42664
11	Tetra thin face-sheet	69.89168	27.537	19.89169
12	Tetra thick pin	80.94521	69.199	24.96958

Table 7. Average transmission loss values for various designs

thickening the face-sheets is comparable to increasing the face-sheet density. This suggests that the mass of the face-sheets has a more dominant effect on the transmission loss value than the thickness of the face-sheets in this case. By inspecting the frequency response results of these cases, it was found that the higher mode resonant frequencies varied by a greater amount as the mass of the face-sheet is increased to a higher value, and the lighter face-sheet is less sensitive at higher frequencies in terms of resonant frequency. These examples of how the attributes of the face-sheet affect the acoustic and structural properties can be used to optimize required structural

strength of a TCS panel, the allowable transmitted noise, and the resonance frequencies of the structure. However, the change in face-sheet properties will affect the mass properties of a TCS structure significantly, and therefore care should be taken when modifying the design parameters associated with the face-sheet so that the weight is minimized for structural purposes.

The finite element analyses used beam structures to investigate the acoustic and structural characteristics of TCS structures so that the various design parameters related to a TCS panel can be tailored to provide adequate sound insulation needed for an aircraft cabin. Although the basic characteristics of a TCS panel are similar to a TCS beam, the acoustic response and performance can be different. Therefore, experiments were carried out in order to validate the assumptions made regarding the relationships between TCS beam and panel, as well as to give a quantitative measure of transmission loss that TCS structures are capable of providing. The FEA results showed that the pyramid and the tetrahedral unit cell designs provided the highest difference in terms of modal density within the frequency range of interest, while the fabrication of these two designs is relatively manageable using the facilities at UTIAS. Therefore, it was decided that two panels would be made using these designs. A low-volume, cost-effective fabrication technique was developed in order to build TCS panels for acoustic chamber testing for evaluating their transmission-loss properties. The panels were constructed using fixtures designed to provide sufficient accuracy for fabricating multiple TCS panels that are representative of the FEA models. The weights of the panels are 1.106 kg and 1.474 kg; the corresponding panel densities are 0.226 g/cm^3 and 0.301 g/cm^3, and the areal densities are 0.361 g/cm^2 and 0.542 g/cm^2 for the tetrahedral and the pyramidal unit cell design TCS panels respectively. The pyramidal unit cell TCS panel has an average of 12% higher transmission loss than the tetrahedral unit cell TCS panel. Part of the difference is due to the mass difference between the two panels, which is mainly due to the mixture of the residual foam and cured resin. FEA results showed a similar trend. The pyramid unit cell panel has an average of 9% higher transmission loss than the tetrahedral unit cell design. In the FEA model, there is a prominent drop in transmission loss for the tetrahedral unit cell design beam at 3150 Hz, which is due to the resonant frequency observed in the spectrum analysis and the lack of damping.

Although the FEA showed the general trend of the transmission loss of two TCS beams, the magnitude and the characteristics of the transmission loss is different from the acoustic chamber experiments. This is due to the fundamental difference between a beam, which is used

in the FEA, and a panel, which is used in the experiment. The boundary conditions between the two cases were different, and the vibration response of a structure is strongly dependent on the boundary conditions, therefore the response between the two cases should be different. In addition, certain vibration modes on a panel do not have a counterpart on a beam, thus certain natural frequencies that occur in a panel analysis do not appear in a beam analysis. Despite the discrepancies between the TCS beam and panel analyses, the TCS beam analyses identified a number important trends regarding the various design parameters associated with TCS structures. The design parameters that were explored in this research include unit cell design, pin angle, pin diameter, core density, face-sheet density, face-sheet thickness, and unit cell spatial distribution. The acoustic performance trends of these parameters are similar in TCS beam and panel analyses because the governing equations in elasticity and vibration for a beam and panel are similar. Also, this is evident from the acoustic chamber experiment when the same unit cell designs were used in both the beam models and the TCS panels. From these comparisons, it can be concluded that the FEA models of TCS beam structures are capable of providing the performance trend of a TCS panel structure, and the acoustic properties of a TCS panel can be significantly controlled by the structure of its unit cell truss design.

Chapter 6

Recommendations

The results obtained from this research provided a valuable tool to design TCS structure for noise mitigation purposes. The FEA results revealed how the various design parameters can affect the acoustic characteristics of a TCS structure. The acoustic chamber experiment results confirmed the FEA findings, and showed that a beam model analysis can demonstrate a number of important acoustic performance trends of TCS panel structures, such as transmission loss (TL), modal densities, and spectrum intensities.

Testing showed that damping may be a beneficial characteristic for the panel by coating damping material on the surface of the carbon pultruded rods. For this reason, the effect of damping should be explored further using FEA models by incorporating energy dissipating mechanisms in the models. In the present development, the mixture of polystyrene foam and the cured resin provided the major source of damping. However, a more weight efficient and cohesively stable material should be used to achieve the same effect as shown in the experiments, which is the relatively steady increase or decrease of TL values across the entire frequency range of interest.

Although the finite element beam model was capable of providing insights regarding the design of a TCS panel, there are design parameters that a beam model is not capable to address. Some of these design parameters include boundary conditions, various plate excitation modes, the effect of fabrication errors, etc. The boundary conditions have a significant effect on the panel's response to acoustic load, and the result of such analysis can provide important information on how to install these panels most efficiently in an aircraft structure. Also, there are certain plate vibration modes that do not have a similar mode in a beam model, one such example is twisting. Therefore a panel model is required to model these phenomena. It is recommended that a panel model should be used in further investigation effort. In addition, the

present FEA beam models did not include fabrication errors, such as incorrect pin angles, localized joint failure at the pin, and localized damages on the face-sheet, therefore they are incapable to provide insight regarding the manufacturing aspect of TCS panels. A more robust model that includes possible fabrication errors can provide much insight into the requirement of manufacturing tolerances and quality control issues.

The methods developed in this research to fabricate a TCS panel are extremely time-consuming. A single panel requires around 250 hours of labour to complete, which seriously limited the number of panels that can be tested in an acoustic chamber. It is recommended that a more automated pin insertion process be developed in order to improve the fabrication time and the consistence of the TCS unit cell structure in the panel. In addition, smaller scale TCS panel should be fabricated in order to explore the various aspects of the manufacturing issues. Some of these issues include excess resin in the foam core, maintaining the proper thickness of the panel, and incomplete saturation of the composite fabric. These issues should be addressed before a full size TCS panel is fabricated.

Bibliography

[1] W.R. Graham. Boundary layer noise and vibration, PhD Thesis, Cambridge University Engineering Department, 1993

[2] W.V. Bhat. Flight test measurement of measurement of exterior turbulent boundary layer pressure fluctuations on Boeing Model 737 airplane, Journal of Sound and Vibration, 1971

[3] W.V. Bhat and J.F. Wilby. Interior noise radiated by an airplane fuselage subjected to turbulent boundary layer excitation and evaluation of noise reduction treatments, Journal of Sound and Vibration, 1971

[4] G.P. Gibbs, R.H. Cabell and J. Juang. Controller Complexity for Active Control of Turbulent Boundary-Layer Noise from Panels, AIAA Journal, 2004

[5] Don E. Bray. Turbulent-boundary-layer noise in the interior of aircraft operating at varying altitudes, Journal of Acoustical Society of America, 1976

[6] H.S. Ribner. Boundary-Layer-Induced Noise in the interior of Aircraft, Institute of Aerophysics, Toronto, April 1956

[7] Dr Michael Bagshaw. An Investigation of Unilateral Hearing Loss amongst Professional Flight Crew, Head of Occupational and Aviation Medicine, British Airways, April 2011

[8] C. H. Hansen. Active Control of Noise and Vibration, Department of Mechanical Engineering, University of Adelaide, South Australia, 1991

[9] S. M. Kuo, and D. R. Morgan. Active Noise Control Systems – Algorithms and DSP Implementations, Wiley, New York, 1996

[10] Li et al. Mechanical Response of All-composite Pyramidal Lattice Truss Core Sandwich Structures, Journal of Material Science Technology, 2011

[11] J.C. Wallach and L.J. Gibson. Mechanical Behaviour of a Three-Dimensional Truss Material, International Journal of Solid and Structures, 2001

[12] V.S. Desphande, N.A. Fleck. Collapse of Truss Core Sandwich Beams in 3-Point Bending, International Journal of Solid and Structures, April 2001

[13] S. Chiras et al. The Structural Performance of Near-Optimized Truss Core Panels, International Journal of Solid and Structures, 2002

[14] N. Wicks, J.W. Hutchinson. Optimal Truss Plates, International Journal of Solids and Structure, 2001

[15] N. Wicks, J.W. Hutchinson. Performance of Sandwich Plates with Truss Cores, Journal of Mechanics of Materials, 2004

[16] H. Bart-Smith, F. Cote, R. Biagi, V.S. Deshpande. Structural response of pyramidal core sandwich columns, International Journal of Solid and Structures, May 2007

[17] S. Hyun, S. Torquato. Optimal and Manufacturable two-dimensional, Kagome-like Cellular Solids, Journal of Materials Research, 2002

[18] S. Hyun, A.M. Karlsson, S. Torquato, A.G. Evans. Simulated Properties of Kagome and Tetrgonal Truss Core Panel", 2003, International Journal of Solids and Structures, 40, 6989-6998

[19] J. Wang, A.G. Evans, K. Dharmasena, H.N.G. Wadley. On the Performance of Truss Panels with Kagome Cores, International Journal of Solids and Structures, 2003

[20] J.H. Lim, K.J. Kang. Mechanical Behaviour of Sandwich Panels with Tetrahedral and Kagome Truss Cores Fabricated from Wires, International Journal of Solids and Structures, 2006

[21] G. Kurtze, B.G. Watters. New Wall Design for High Transmission Loss or High Damping, Journal of Acoustical Society of America, 1959

[22] M.A. Lang, C.L. Dym. Optimal Acoustic Design of Sandwich Panels, Journal of Acoustical Society of America, 1975

[23] C.K. Barton, J.S. Mixon. Noise Transmission and Control for Light Twin-Engine Aircraft, Journal of Aircraft, 1981

[24] F.W. Grosveld, J.S. Mixson. Noise Transmission Though an Acoustically Treated and Honeycomb-Stiffened Aircraft Sidewall, Journal of Aircraft, 1985,

[25] J.A. Moore, R.H. Lyon. Mode Canceling Panel for Greater Than Mass-Law Transmission Loss in the Principal Speech Bands, U.S. Patent No. 4,106,588, 1978

[26] P. Thamburaj, Q. Sun. Optimization of Anisotropic Sandwich Beams for Higher Sound Transmission Loss, Journal of Sound and Vibrations, 2002

[27] M. El-Raheb. Frequeny Response of a Two-Dimensional Trusslike Periodic Panel, Journal of Acoustical Society of America, 1997

[28] M. Ruzzene, F. Scarpa, F. Soranna. Wave Beaming Effects in Two-Dimensional Cellular Structures, Smart Material Structure, 2004

[29] M. El-Raheb, P. Wagner. Transmission of Sound Across a Trusslike Periodic Panel; 2-D Analysis, Journal of Acoustical Society of America, 1997

[30] A. Spadoni, M. Ruzzene. Structural and Acoustic Behavior of Chiral Truss-Core Beams, 2006

[31] S.P. Crane, K.A. Cunefare, S.P. Engelstad, E.A. Powell. A Comparison of Optimization Formulations for Design Minimization of Aircraft Interior Noise, Journal of Aircraft, 1997

[32] K.A. Cunefare, B. Dater. Structural Acoustic Optimization Using the Complex Method, Journal of Computational Acoustics, 2003

[33] G. Corcos. Resolution of Pressure in Turbulence, Journal of the Acoustical Society of America, 1963

[34] G. Corcos. The Structure of the Turbulent Pressure Field in Boundary Layer Flows, Journal of Fluid Mechanics – Cambridge Journal Online, 1964

[35] B.M. Efimtsov. Characteristics of the Field of Turbulent Wall Pressure Fluctuations at Large Reynolds Numbers, Soviet Physics Acoustics, 1982

[36] D.A. Bies. A Review of Flight and Wind Tunnel Measurements of Boundary Layer Pressure Fluctuations and Induced Structural Reponse, NASA CR-626, 1966

[37] R. Wahidi, W. Chakroun, S. Al-Fahed. The Behavior of the Skin Friction Coefficient of a Turbulent Boundary Layer Flow over a Flat Plate with Differently Configured Transverse Square Grooves, Experimental Thermal and Fluid Science, 2005

[38] J.D. Rocha, A. Suleman, F. Lau. An Accurate Coupled Structural-Acoustic Analytical Framework for the Prediction of Random and Flow-Induced Noise in Transport Vehicles: Its Validation, Journal of Vibrations and Acoustics, 2011

[39] A. Berry, J.L. Guyader, J. Nicolas. A General Formulation for the Sound Radiation from Rectangular, Baffled Plates with Arbitrary Boundary Conditions, Journal of Acoustical Society of America, 1990

[40] F. Fank, P. Gardonio. Sound and Structural Vibration – Radiation, Transmission and Response, Elsevier, 2006

[41] C.E. Wallace. Radiation Resistance of a Rectangular Panel, Journal of Acoustical Society of America, 1972

[42] K.F. Graff. Wave Motions in Elastic Solids, Dover Edition, 1991

[43] A. Spadoni, M. Ruzzene. Structural and Acoustic Behavior of Chiral Truss-Core Beams", ASME, 2006